

Aggregation and transport behaviour of sediment surface particles in Mecklenburg Bight, south-western Baltic Sea, affected by biogenic stickiness

Aggregation und Transportverhalten von Oberflächensedimenten der Mecklenburger Bucht (süd-westliche Ostsee) unter besonderer Betrachtung biogener Klebrigkeit

Dissertation zur Erlangung des akademischen Grades doctor rerum naturalium (Dr. rer. nat.) der Mathematisch-Naturwissenschaftlichen Fakultät der Universität Rostock

vorgelegt von Kai Ziervogel

Rostock, im September 2003

Die vorliegende Arbeit wurde von der Mathematisch-Naturwissenschaftlichen Fakultät der Universität Rostock als Dissertation angenommen und am 15. Dezember 2003 erfolgreich verteidigt.

Die Gutachter waren: Prof. Dr. Gerhard Graf, Universität Rostock
Prof. Dr. Jan Harff, Universität Greifswald
Prof. Dr. Karin Lochte, Universität Kiel

Table of contents

Zusammenfassung	5
Introduction	7
Study area	12
Material and methods	15
Sediment sampling and erosion experiments	15
Erosion device microcosm	15
Critical shear stress velocities derived from microcosm experiments ($u^*_{cr-initial}$ and $u^*_{cr-erosion}$)	17
Critical shear stress velocity calculated from Shields parameter ($u^*_{cr-Shields}$)	19
Critical shear stress velocity calculated from Hjulström curve ($u^*_{cr-Hjulström}$)	20
Critical shear stress velocity calculated from flow velocities ($u^*_{cr-flow}$)	21
Analysis of sediment parameters	24
Chlorophyll <i>a</i> equivalents (<i>Chl</i>)	24
Carbohydrate equivalents (<i>CHE</i>)	26
Benthic diatom abundance	26
Irradiance measurements	26
Roller table experiments	27
Experimental setup	27
Water samples	31
Total suspended particulate matter (<i>SPM</i>)	31
Chlorophyll <i>a</i> equivalents (<i>Chl</i>)	31
Particulate organic carbon and nitrogen (<i>POC</i> and <i>PON</i>)	31
Biogenic sticky particles (<i>CHE</i> and <i>TEP</i>)	32
Bacteria and diatom abundance	33
Statistical analysis	33
Results	35
Erosion experiments	35
Mud cores	35
Fine sand cores	35
Erosion thresholds compared to calculated u^* values	37

Sediment parameter	40
<i>Col S, Col EDTA, Chl</i>	40
Diatom abundances	42
Correlation of sediment parameter and erosion thresholds	43
Irradiance measurements (<i>PAR</i>)	45
Aggregate formation and sinking behaviour of resuspended particles	46
Aggregate formation	46
Sinking velocities	49
Particle analysis	51
Algae and bacteria cell abundance	53
Discussion	54
Determination of erosion thresholds – a critical examination	54
Sediment erosion in the study area	56
Variations of erosion thresholds and micro-biostabilisation effects	58
Aggregation behaviour of resuspended particles	65
Settling velocities and particle residence time in the <i>BBL</i>	67
Pathways of resuspended particles (resuspension loops)	69
Summary	74
Literature	76
Danksagung	91
Erklärung	92
Lebenslauf	93

Zusammenfassung

Ziel der vorliegenden Arbeit war es die Prozesse der Erosion von Sedimentpartikeln sowie das Aggregations- und Transportverhalten der Partikel in der Wassersäule zu beschreiben. Dabei wurde besonders der Einfluss exopolymerer Substanzen, die von pelagischen (*TEP*) und benthischen Organismen (*EPS*) produziert werden, berücksichtigt. Die Beprobung der Sedimentoberflächen wurde an zwei Stationen der Mecklenburger Bucht durchgeführt. Die Feinsandstation in Küstennähe hatte eine Wassertiefe von 19 m. Im Becken der Mecklenburger Bucht, in einer Wassertiefe von 25 m, wurden Schlickproben gewonnen. Die Sedimenttypen „Feinsand“ und „Schlick“ bedecken zusammen etwa 80% des Meeresbodens im Probennahmegebiet und sind daher die dominanten Sedimenttypen.

Erosionsexperimente wurden mit der Erosionskammer Mikrokosmos an fünf verschiedenen Zeitpunkten im Jahr durchgeführt. Dabei wurden zwei Schwellenwerte für den Partikeltransport definiert ($u^*_{cr-initial}$ und $u^*_{cr-erosion}$), welche über den Zeitraum der Probennahme an beiden Stationen signifikant positiv miteinander korrelierten.

An der Schlickstation beeinflusste eine unkonsolidierte Sedimentauflage (Fluff) den Sedimenttransport zu jedem Zeitpunkt der Probennahme. In geringerem Maße bedeckte diese auch die Sedimente der Feinsandstation. Hier lagen die mittleren Werte von $u^*_{cr-erosion}$ bei 1.2 cm s^{-1} und damit im Bereich von Literaturdaten ($u^*_{cr-Shields}$ und $u^*_{cr-Hjulström}$), deren Berechnungen sich auf die Korngröße beziehen. An zwei Probennahmezeitpunkten verringerte eine stärker ausgeprägte Fluffauflage die kritischen Schubspannungsgeschwindigkeiten. Da die hier präsentierten und aus der Literatur bekannten kritischen Schubspannungsgeschwindigkeiten für Fluff bei $\leq 1.0 \text{ cm s}^{-1}$ liegen, kann dieser Wert als ein einheitlicher Schwellenwert angesehen werden, der eine Identifikation von Fluffauflagen über das Erosionsverhalten ermöglicht. Betrachtet man den Massentransport von partikulärem Material in die

Wassersäule, so nimmt der Transport von Fluff im Untersuchungsgebiet in diesem Zusammenhang eine dominante Rolle ein.

Während des gesamten Probennahmezeitraumes von September 2000 bis Januar 2002 variierten die Erosionsschwellenwerte an der flacheren Feinsandstation um den Faktor 2.4. An der Schlickstation wurden Variationen um den Faktor 2 gemessen. Die Konzentrationen wasserlöslicher, kolloidaler Kohlenhydrate (*Col S*), die als Indikator für *EPS* gelten, korrelierten positiv mit $u_{cr-erosion}^*$. Jedoch konnten die Quellen der Kohlenhydrate nicht identifiziert werden. Die gemessenen und berechneten Lichtverhältnisse an den untersuchten Stationen verdeutlichen, dass Netto-Photosynthese und Produktion von Exsudaten auf ruhige Wetterlagen mit optimalen Lichtverhältnissen beschränkt sind. Effekte der Mikro-Biostabilisation sind hingegen auf Flachwasserregionen mit Wassertiefen <5 m beschränkt, da in diesen geringen Tiefen Lichtintensitäten erreicht werden, die phototrophes Wachstum ermöglichen ($>5 - 10 \mu E m^{-2} s^{-1}$). Daraus folgt, dass nur etwa 10% der Sedimentoberflächen in der Mecklenburger Bucht von Mikro-Biostabilisationseffekten beeinflusst werden können.

Die an Partikel gebundenen benthischen Diatomeen interagieren in der bodennahen Wassersäule mit organischem Material sowie mit Mineralen und bilden makroskopische Aggregate. Eine hohe Aggregationseffizienz konnte experimentell in einer Suspension natürlicher Sedimentpartikel mit zugefügten Zellen einer pelagischen Algenkultur (*Skeletonema costatum*) nachgewiesen werden. Ohne die Zellen der Algenkultur zeigte das Material mit natürlicher Mikroorganismengemeinschaft eine geringere Aggregationseffizienz. Darüber hinaus wiesen *S. costatum* Aggregate höhere Sinkgeschwindigkeiten (W_{s-exp} und W_{s-cal}) und verglichen mit den Aggregaten ohne *S. costatum* die doppelte Anzahl benthischer Algenzellen vor. Für Aggregate mit geringeren biologischen Komponenten wurden daher 3-fach höhere Residenzzeiten berechnet. Diese waren jedoch um mehrere Zehnerpotenzen geringer, als aus der Literatur bekannte Residenzzeiten.

S. costatum Aggregate durchlaufen auf ihrem Weg von der Küste in die Becken eine hohe Anzahl an Resuspensions- und Depositionsschleifen. Benthische Diatomeen, die an beiden Stationen im Oberflächensediment gefunden wurden werden in den Aggregaten lateral transportiert. Dies kann gesteigerte Interaktionen mit dem Benthos,

sowie eine längere Retention organischen Materials in Küstensedimenten zur Folge haben.

Introduction

The top layer of coastal sediments constitutes a dynamic system with regard to exchange processes of dissolved and particulate materials. The processes involved in sediment transport are of great concern to sedimentological and biological research. Modelling sediment transport gains importance because coastal environments are exposed to increasing stress for instance through dredging and dumping of dredged material. In this context, the influence of biota on sediment stability and the response of the benthic and pelagic environment to erosion becomes a fundamental interest (Krumbein et al. 1994).

Erosion [lat. *erosio*] is defined as subaerial corrosion due to wind, ice and water forces. In aquatic systems, rolling transport of single grains and particle entrainment influences biological and biogeochemical exchange processes between the sediment surface and the overlying water. It has to be seen as a complex process being affected by benthic micro-, meio- and macrofauna and morphological (grain size) and physico-chemical properties (temperature, salinity, pH, water content, porosity, mineralogy) of the sediment (Paterson and Black 1999).

Research on sediment dynamics and erosion has a long tradition, starting with the classic studies of Hjulström (1935) and Shields (1936); summaries can be found e.g. in Miller et al. (1977) and Soulsby (1997). These studies, correlating grain size with flow velocity that exerts a friction force on the bed, postulate the existence of a threshold value which determines the initial movement of particles (incipient motion). This value can be described as critical shear stress (τ_{cr} [N m⁻²]) or critical shear stress velocity (u_{cr}^* [m s⁻¹): $\tau_{cr} = u_{cr}^{*2} \rho$, where ρ is the fluid density [kg cm⁻³]. Different *in situ* and laboratory erosion devices are used (see Black and Paterson 1997 for a review) to

measure critical shear stress velocities by subjective methods, e.g. visual observation or by the measurement of erosion flux, i.e. the mass of suspended particulate matter (*SPM*) being entrained from an area of the sediment surface over a period of time ($\text{kg m}^{-2} \text{s}^{-1}$).

However, resuspension curves based solely on sedimentological parameters do not adequately describe transport processes in natural, inhabited sediments. The biogenic influence on sediment erosion has to be considered and has been intensively studied in the past (see Widdows and Brinsley 2002 for a review). Direct and indirect deposition and resuspension of particles as well as bioturbation of benthic organisms are important processes to address in the research of biostabilisation and –destabilisation of sediment surfaces (Graf and Rosenberg 1997). A functional grouping of organisms as stabilisers and destabilisers was found to be impractical (Jumars and Nowell 1984). One example of benthic invertebrates belonging to both groups is the amphipod *Corophium volutator*. While several authors described destabilisation effects due to bioturbation (Daborn et al. 1993, Gerdol and Hughes 1994) and bioresuspension activities (De Deckere et al. 2000), others illustrated the production of mucus resulting in stabilisation of sediment surfaces (Meadows and Tait 1989, Mouritsen et al. 1998).

Numerous authors studying erosion on natural (Grant et al. 1986, Grant et al. 1986 b, De Jonge and Van den Bergen 1987, Grant and Bathmann 1987, Grant and Gust 1987, Riethmueller et al. 2000) and artificial sediment surfaces (Holland et al. 1974, Dade et al. 1990, Paterson 1990, Meadows et al. 1994), postulate an important role of benthic diatoms in stabilising cohesive and non-cohesive sediments, especially on intertidal mudflats (e.g. Krumbein et al. 1994, Paterson and Black 1999 for reviews).

Microbial biofilms are widespread in aquatic environments. Diatoms (*Bacillariophyceae*) producing exopolymeric substances (*EPS*) were found to dominate these assemblages in the upper layers of light saturated, coastal sediments (Jørgensen and Revsbech 1983). *EPS* mainly consisting of polysaccharide molecules (Decho 2000) are secreted through a cell structure (the raphe) when a diatom cell is actively moving (Edgar and Pickett-Heaps 1984). These exudates are thought to be responsible for gluing sediment particles together and thus, increasing sediment cohesion and erosion resistance of sediment surfaces. Underwood et al. (1995) suggested an extraction

procedure of sediment carbohydrates for the quantification of *EPS* equivalents. The relationship between the content of biogenic exudates in the sediment and benthic diatom biomass remained difficult because of the great variety of carbohydrate sources in aquatic environments (Decho 1990).

In contrast to the extensive work on intertidal mudflats concerning stabilisation by microorganisms, micro-biostabilisation, less is known about the influence of microalgae on the stability of subtidal sediments. Several compilations outlined the importance of benthic diatoms for primary production in a wide range of aquatic environments with varying water depths (e.g. Mac Intyre et al. 1996, Cahoon 1999). Recently, benthic diatom mats were found in a water depth of 30 m significantly contributing to net photosynthesis (Glud et al. 2002). Furthermore, there is some evidence in the literature of benthic diatoms building biofilms and influencing sediment stability in areas lacking a regular tidal emersion (Madsen et al. 1993, Lund-Hansen et al. 2002).

Following resuspension, the pathways of particle transport are specified as deposition as well as aggregation and disaggregation processes. Generally, the formation of macroscopic aggregates in the water and the subsequent sedimentation to the sea floor leads to an enhanced vertical transport of organic and inorganic particulate matter (Fowler and Knauer 1986). Especially after diatom blooms, aggregates were found to settle out of the euphotic zone of the water column (Alldredge and Silver 1988). After sedimentation, aggregates form an unconsolidated, fluffy surface layer at the sediment-water interface (Stolzenbach et al. 1992, see Beaulieu 2002 for a review). Recent studies suggest that resuspension and lateral transport of aggregates are major compounds influencing aggregate formation and transport processes in the *BBL* (Jähmlich et al. 1999, Jähmlich et al. 2002). Fluff is characterised by loosely bound components that were found to be resuspended into the benthic boundary layer (*BBL*) at relatively low current velocities (Beaulieu 2003).

The processes leading to aggregate formation in the water column have been studied extensively (see Simon et al. 2002 for a review). Briefly, particle aggregation is controlled by collision rate and collision efficiency of particles, which in turn is controlled by stickiness. Three mechanisms are used to describe the former process: Brownian motion, shear and differential settlement (Jackson 1990). Collision efficiency

may vary with particle shape and type and the geochemical properties of the particle surface, e.g. particle stickiness of microorganisms. Pelagic diatoms show sticky cell surface coating and, therefore, form aggregates in the water column by coagulation. This process has been demonstrated by numerous laboratory and field experiments (e.g. Smetacek 1985, Kioerboe et al. 1990). Furthermore, dissolved polysaccharides exuded from pelagic microorganisms coagulate in the water column, forming transparent exopolymer particles (*TEP*) via cationic bridging between polysaccharide fibrils (Alldredge et al. 1993). *TEP* particles influence aggregation and sedimentation of diatom blooms (Passow et al. 1994, Passow & Alldredge 1995). Recently, bacterioplankton capsular material released into the ambient water has been found to contribute significantly to the oceanic *DOC* pool and after coagulation, to the *TEP* pool (Stoderegger and Herndl 1998, Stoderegger and Herndl 1999).

The influence of benthic microorganisms on particle aggregation in the *BBL* remains unravelled. Nevertheless, numerous authors measured increasing concentrations of photopigments in bottom waters after sediment resuspension containing benthic diatoms (Grant and Bathmann 1987, Grant and Gust 1987, Wiltshire et al. 1998) indicating a simultaneous resuspension of sticky particles. In subtidal areas diatoms are found to be abundant in unconsolidated, fluffy surface layers (Lund-Hansen et al 2002). Therefore, the potential for sticky microorganisms to be resuspended into the *BBL* is apparently high.

The central aim of this study was to investigate the influence of microorganisms on transport processes of sediment particles in Mecklenburg Bight, south-western Baltic Sea. Next to the sedimentological influence on sediment erosion, effects of microorganisms on particle entrainment into the *BBL* as well as aggregation and sinking behaviour were major concerns of the present study. Pathways of particulate matter from the sediment surface into the overlying water are illustrated in figure 1.

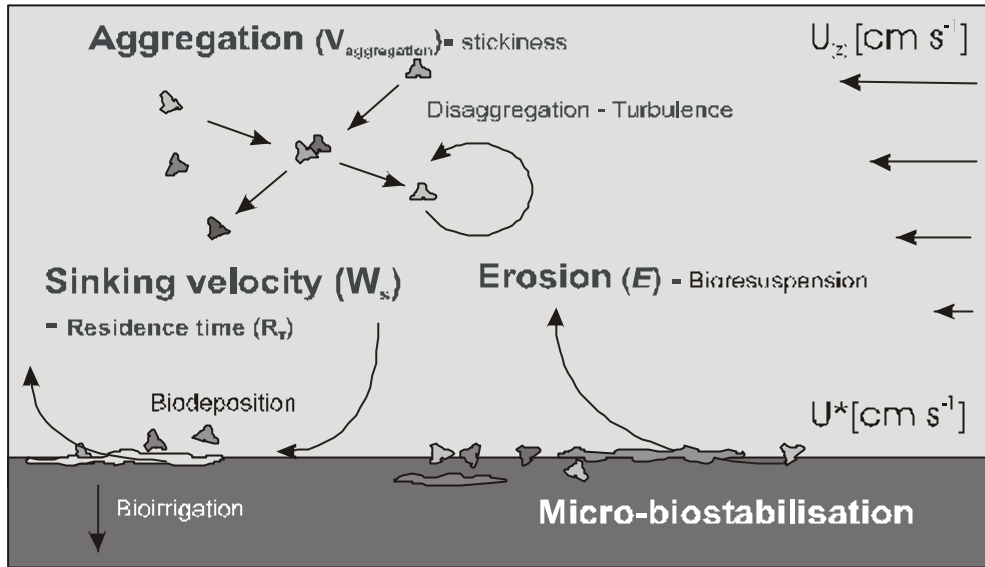


Fig. 1: Illustration of processes influencing particle transport from the seafloor into the water column. Processes written in bold letters are of major concern of the present study.

Resuspension behaviour of natural sediment surfaces and near bed flow conditions were investigated in order to respond to the following questions:

- *Do experimentally derived erosion thresholds of natural sediment surfaces differ from calculated values based on grain sizes measurements?*
- *Do flow velocities predominating in the investigation area induce shear stress velocities adequate to erode sediment surfaces?*

The influence of microorganisms on sediment erosion thresholds as well as transport behaviour in the *BBL* was determined answering the following questions:

- *Do benthic diatoms influence erosion thresholds similarly to light saturated tidal mudflats?*
- *Do assemblages of benthic and pelagic microorganisms effect aggregation kinetics and sinking behaviour of resuspended sediment surface particles?*

Study area

The study area is situated in Mecklenburg Bight, located in the south-western part of the Baltic Sea (Fig. 2). It is one of the largest brackish water bodies on earth with a mean depth of 52 m (HELCOM 1986). Tidal currents are negligible and the general current pattern is subject to considerable variations induced by local weather conditions, wind shear and atmospheric pressure variations over the north-east Atlantic, the North Sea and the Baltic (Dickson 1973).

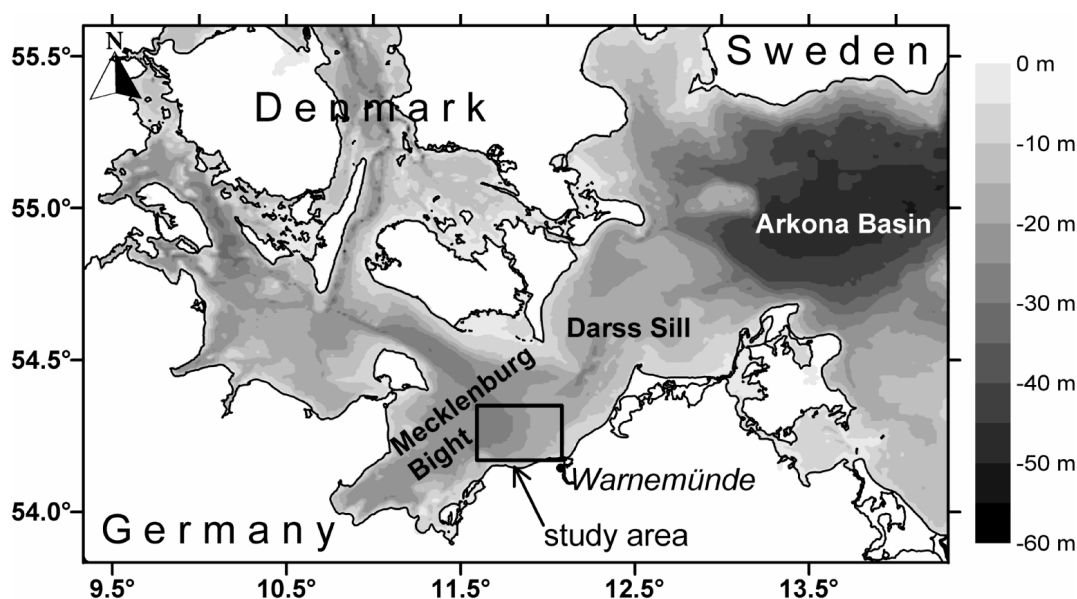


Fig. 2: The study area (rectangle) in Mecklenburg Bight, south-western Baltic Sea. Bathymetric data derived from (Seifert and Kayser 1995).

A meteorological seasonality of the wind and air pressure regime is reflected in a pronounced seasonality of the hydrographic and the biological characteristics within the water column and the sediment (Matthaeus and Nausch 2001). Food supply for the benthos is pronounced by extensive sedimentation of organic rich material after pelagic spring and autumn diatom blooms in coastal waters (Graf 1992). Generally, macrofauna abundance and biomass in Mecklenburg Bight decreases with increasing water depth (Zettler et al. 2000). Highest numbers of macrofauna species were found in the depth zone between 15 and 20 m whereas highest abundance and biomass was detected in

more shallow waters between 5 and 10 m. Muddy areas >25 m with occasionally oxygen deficiency showed lowest species numbers. Less is known concerning microphytobenthos distribution in the study area. Springer (1999) measured sediment chlorophyll *a* concentration indicating algal biomass at water depths >25 m in the study area. Values ranged between 50 and 75 mg m⁻² (recalculated from original data) showing no seasonal variations.

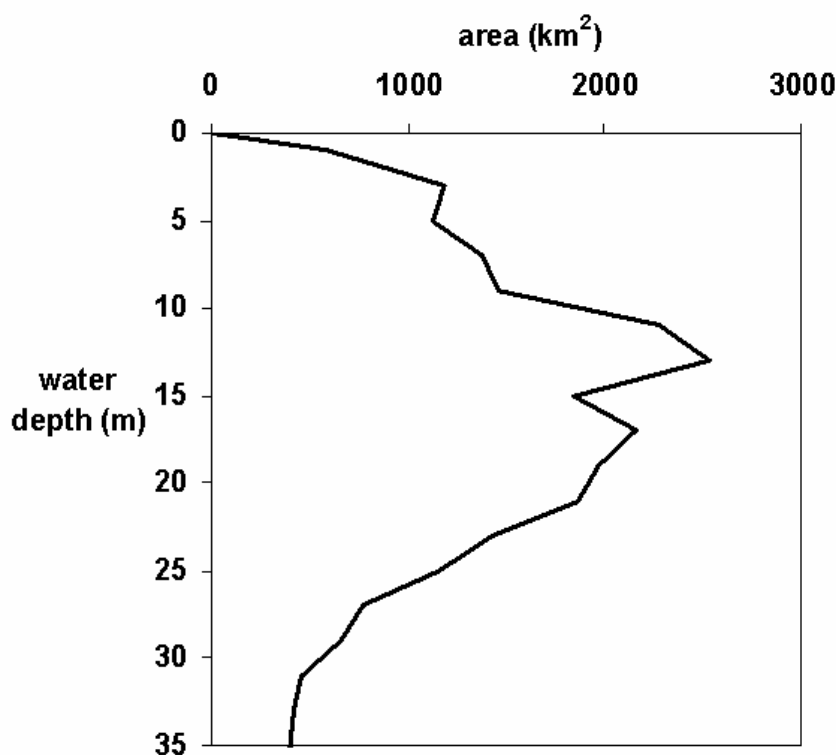


Fig. 3: Hypsographic curve of the study area including Mecklenburg Bight, Arkona Basin and Pomeranian Bight based on bathymetric data from Seifert et al. (2001).

Bathymetric data of Mecklenburg Bight, Arkona Basin and Pomeranian Bight illustrate that areas exceeding 20 m water depth cover approximately 30% of the seafloor (Seifert et al 2001). In these areas, including the central part of Mecklenburg Bight and Arkona Basin, a low-energy hydrodynamic regime results in sedimentation of clay and silt-sized sediment (mud) with grain sizes <63 μm (Lemke et al. 1994). Largest areas are located at water depths of 10 – 15 m (Fig. 3) where fine and medium sands with grain sizes of

125 – 500 μm typically occur (Lemke et al. 1994). Here, near bed flow that is strongly influenced by surface waves predominate in north-easterly directions reaching peak values of 40 cm s^{-1} and a mean velocity of about 10 cm s^{-1} (Leipe pers. comm.).

For this study, sediment samples were collected at two sites (Fig. 3) during five separate cruises in September 2000, April 2001, July 2001, October 2001 and January 2002: a fine sand site with a mean grain size of $132 \mu\text{m}$ and a water depth of 19 m ($54^\circ 12.06' \text{ N}$, $11^\circ 54.24' \text{ E}$) and a mud site with a mean grain size of $21 \mu\text{m}$ and a water depth of 25 m ($54^\circ 13.26' \text{ N}$, $11^\circ 36.96' \text{ E}$).

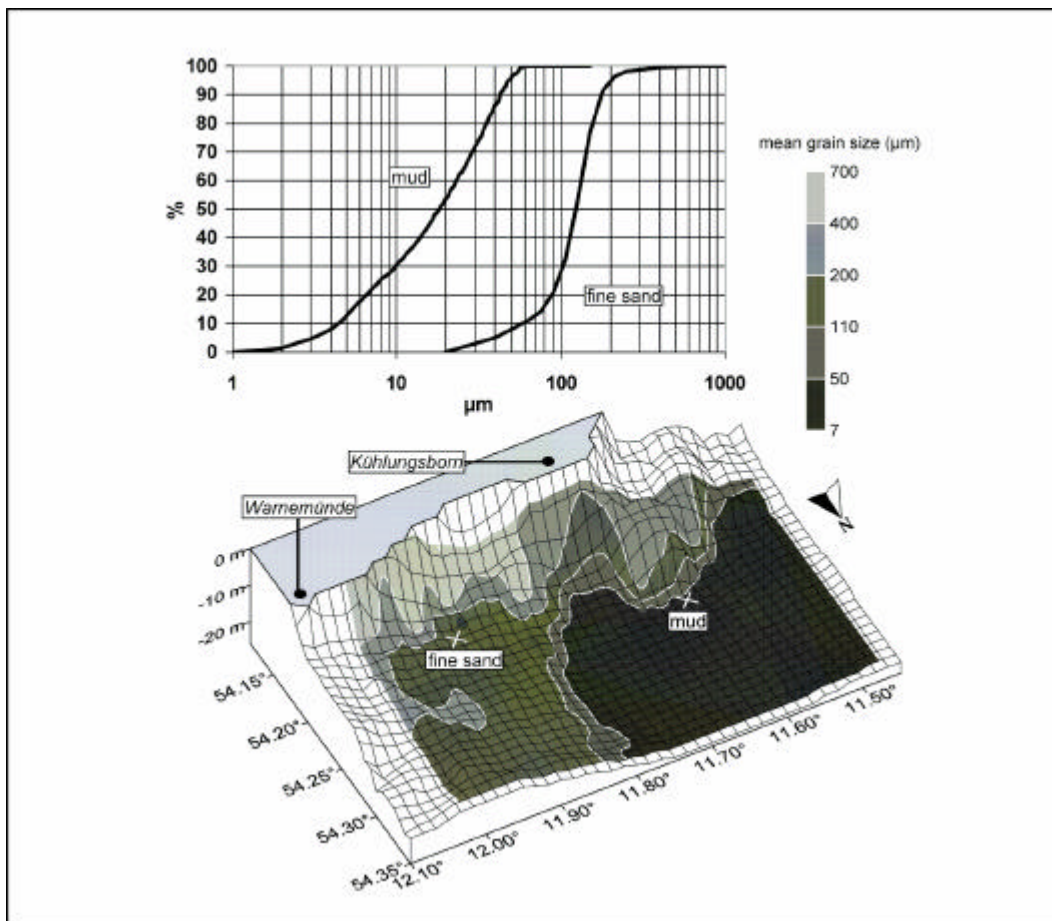


Fig. 4: Grain size distribution of the two selected sites (upper graph) and the study area (lower graph). An area-wide collection of sediment samples from the upper 5 cm ($n = 190$) was conducted by Bohling (2003) who determined sedimentological parameters (for methods see Bohling 2003).

According to Bohling (2003) who mapped sedimentological parameters in the study area (Fig. 4), both sites represent the two dominant sediment types in the area. About 48% of the area is covered by mud that has a mean water content of >50% dry weight (% dw) and an organic content of about 4% dw. On the other hand, fine sand with a mean water content of about 22% dw and less than 0.5% dw organic content covers 28% of the area.

Material and methods

Sediment sampling and erosion experiments

Erosion device microcosm

Cylindrical samples of 20 cm in diameter were taken with a box-corer and erosion experiments were carried out on-board in a erosion device microcosm (Gust and Müller 1997), into which sediment cores and *in situ* seawater (overlying water height 10 cm) were inserted (Fig. 5).

This device consists of a removable lid with a stirring disc and a water input and output. Water was pumped via the central axis of the lid through an external water cycle and back into the overlying water of the core. By controlling the rotational speed of the disc and the pumping rate, the device generates a homogeneous shear stress velocity at the bottom. Bottom shear stress in the erosion chamber was calibrated by Gust and Müller (1997) using skin friction probes.

The shear stress velocity was increased in steps of 0.05 - 0.1 cm s⁻¹ with an exposure time of 10 min. After that period, resuspended particle concentration in the overlying water of the sediment core reached a constant value. Once shear stress velocity is high enough to move particles at the sediment surface, they describe logarithmic spirals towards the centre of the core. In the centre, particles are moved upward and transported through the central axis into the external water cycle. Samples were taken with a syringe

from the external water cycle at the end of each 10 min time interval and filtered onto pre-weighed glass fibre filters (0.7 μm pore size).

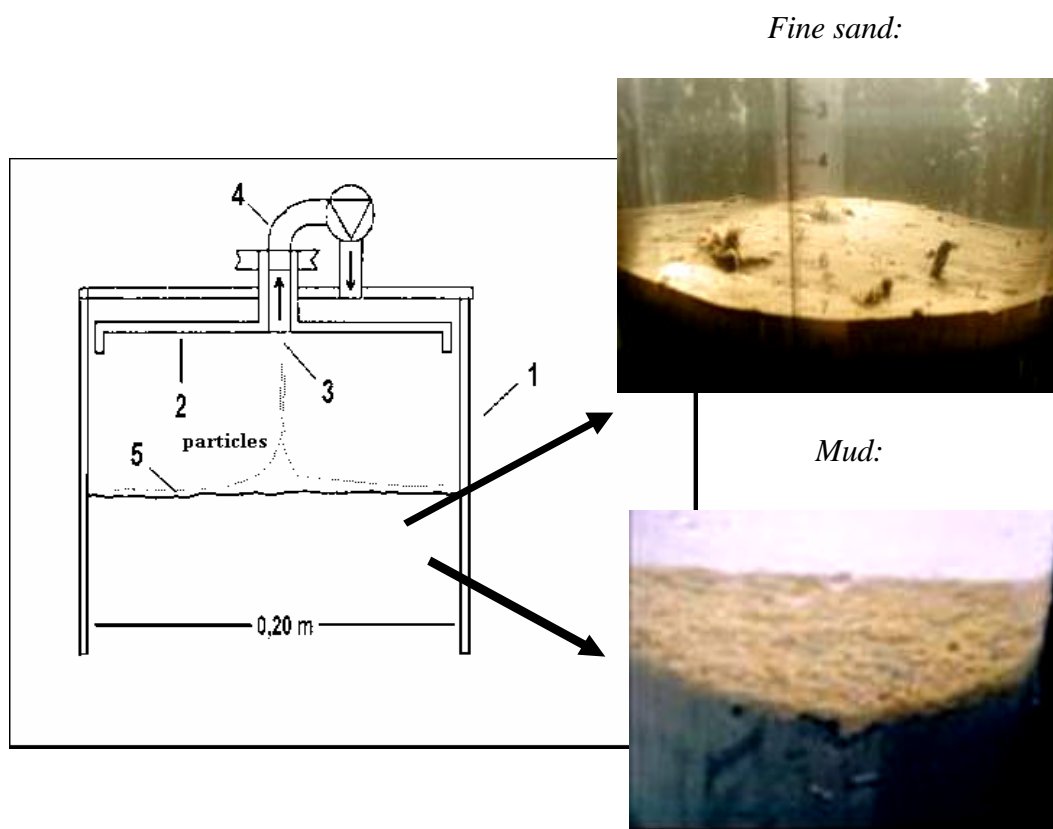


Fig. 5: Cross-section of the erosion device microcosm with (1) sediment core, (2) stirring disc, (3) central axis, (4) external water cycle, (5) sediment surface. Arrows indicate direction of water flow in the external water cycle (redrawn after Gust 1987). Pictures on the right hand side illustrate representative topographies of natural sediment surfaces. Sediment cores taken at the fine sand station were covered by biogenic structures (upper picture) whereas brownish flocs (fluffy layer) characterised the sediment of the mud station (lower picture).

Net erosion flux of surface particles (E) were calculated from the difference in suspended particulate matter concentrations (SPM) before and after shear stress velocity increments using the formula of Tolhurst et al. (2000):

$$E = \frac{1}{A} \frac{SPM(2) - SPM(1)}{t(2) - t(1)} \quad [1]$$

where E is the averaged erosion flux ($\text{kg m}^{-2} \text{s}^{-1}$), A the surface area of the core (m^2), SPM the suspended particulate matter (kg) and t the time (s).

Critical shear stress velocities derived from microcosm experiments

$(u^*_{cr-initial}$ and $u^*_{cr-erosion})$

Two thresholds of critical shear stress velocities were defined differentiating between initial rolling transport of single grains and loosely bound surface material ($u^*_{cr-initial}$), and particle erosion ($u^*_{cr-erosion}$). The former threshold was visually specified when rolling transport of surface particles was detected whereas the latter derived from measurements of SPM being entrained into the overlying water of the investigated sediment cores.

It was possible to make out initial motion of single grains on fine sand but not on mud cores. Here, the threshold of initial particle transport was reached when aggregates of the fluffy surface layer were visibly transported but not yet resuspended. Values of $u^*_{cr-erosion}$ were read off x-axis in diagrams where shear stress velocity increment and flux of particle erosion are plotted (Fig. 12, p. 34). In figure 6, this procedure is illustrated: the value of $u^*_{cr-erosion}$ is reached when erosion (E) increased above a background concentration ($E > 0.5 \cdot 10^{-5} \text{ kg m}^{-2} \text{ s}^{-1}$; horizontal line in the upper graph in Fig. 6). At this value (here: $u^*_{cr-erosion} = 0.4 \text{ cm s}^{-1}$) water turbidity increased indicating particle entrainment into the overlying water of the core (lower graph in Fig. 6). At subcritical shear stress velocity of 0.35 cm s^{-1} , water turbidity increased exponentially to a constant value. At $u^* = 0.4 \text{ cm s}^{-1}$, erosion of sediment particles was characterised by a peak of water turbidity, decreasing to a constant value after 10 minutes incubation time. Without a further increase of shear stress velocity water turbidity would remain at this constant value.

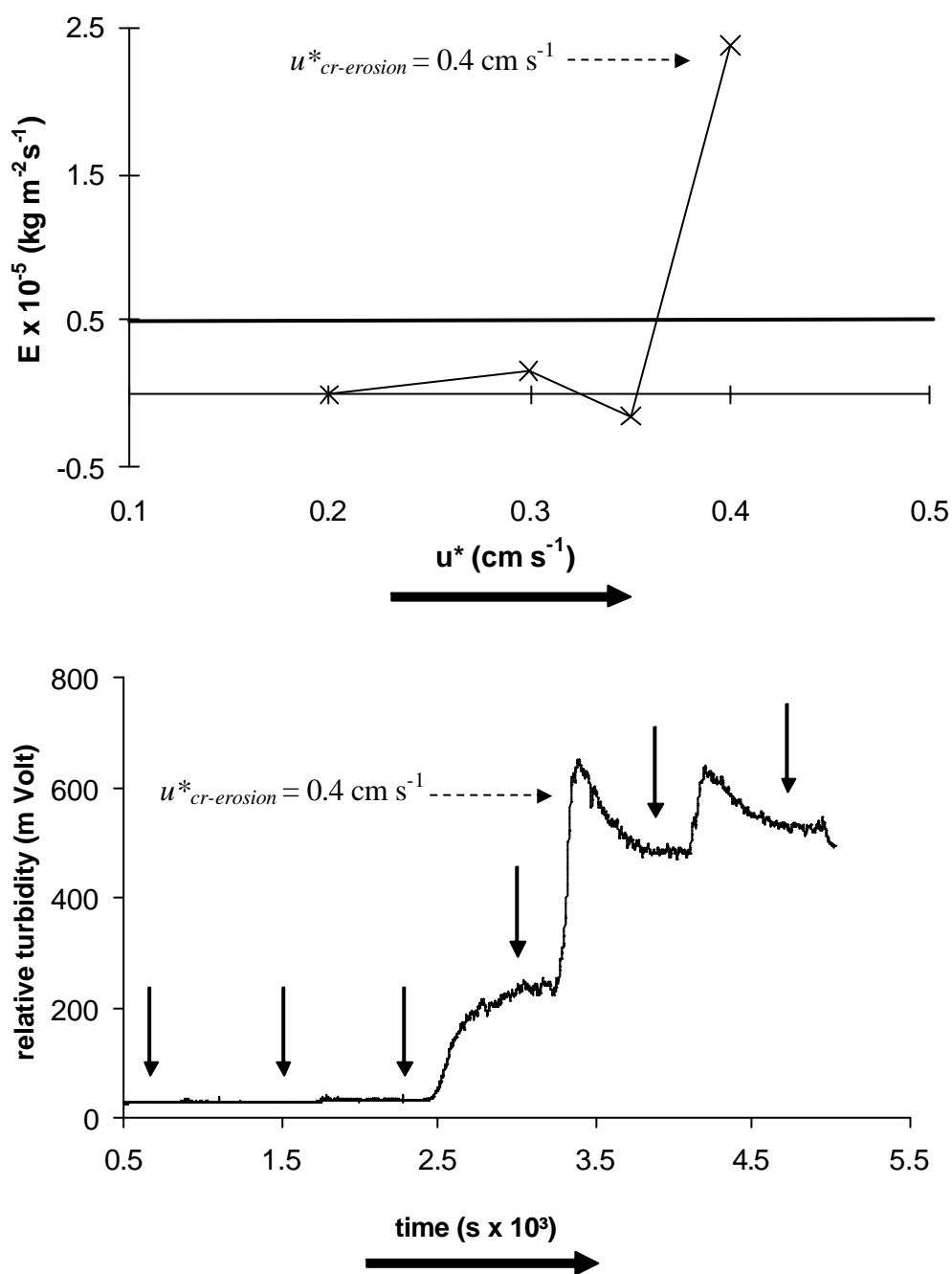


Fig. 6: Erosion experiment with sieved silt sized sediment ($<63 \mu\text{m}$). The upper graph illustrates flux of particle erosion (E) as the differences in SPM concentrations before and after shear stress increments. The horizontal line gives the threshold of E at which $u^*_{cr-erosion}$ is reached (here: 0.4 cm s^{-1}). Negative values of E may indicate particle deposition. The lower graph shows relative turbidity measured in the overlying water of the core during this erosion experiment using the principal of optical backscattering. Arrows indicate shear stress increments.

Particle entrainment occurred in pulses after the initial step for erosion and therefore, values of E can not be projected to timescales >10 min. In order to calculate inventories of mass erosion in the field, a corrected erosion rate by multiplying values of E with 600 was used that refers to the incubation time of shear stress velocities. Nevertheless, according to standard international units, E is expressed as the dry weight of particulate matter (kg) being eroded per square metre and per second.

The threshold value was assessed as the point at which differences in SPM concentrations no longer resulted in negative fluxes. Negative values of E may result from methodological accuracy of reweighing filters (see p. 29). The amount of particles suspended in the overlying water of the cores were low at the beginning of erosion experiments. Thus, calculated differences in SPM concentrations measured at values of u^* lower than $u^*_{cr-erosion}$ may have a negative result. On the other hand, deposition of particles during 10 min incubation time may lead to decreasing particle concentration and thus, negative calculated values of E as discussed by Tolhurst et al. (2000).

Experimentally derived critical thresholds of initial particle transport and erosion were then compared to calculated critical shear stress velocities derived from Shields parameter, Hjulström curve, and measured as well as modelled flow velocities (Tab.1, p. 21).

Critical shear stress velocity calculated from Shields parameter ($u^*_{cr-Shields}$)

Soulsby and Whitehouse (1997) suggested a fit to a corrected Shields curve to calculate the threshold Shields parameter q_{cr} (dimensionless) for cohesionless grains:

$$q_{cr} = \frac{0.3}{1 + 1.2D_*} + 0.055(1 - \exp[-0.020D_*]) \quad [2]$$

$$\text{with } D_* = \left(\frac{gR'}{u^2} \right)^{1/3} d, \text{ where } R' = \frac{(r_s - r_w)}{r_w}.$$

D_* is the dimensionless grain size given by: r' the relative density (sediment particles in relation to density of water, here: 1.6), g the gravitation constant (9.81 m s^{-2}), d the mean grain size (m), and \mathbf{u} the viscosity of water ($10^{-6} \text{ m}^2 \text{ s}^{-1}$). The relative density r' is given by: r_s the density of sediment (2650 kg m^{-3} for quartz sand - most common mineral in marine sands), r_w the density of water (1018 kg m^{-3} for Baltic Sea water).

With the Shields parameter the theoretical critical shear stress velocity can be calculated as follows (dashed line in Fig. 13, p. 36):

$$u^*_{cr-Shields} = \sqrt{\frac{\mathbf{q}_{cr} g (r_s - r_w) d}{r_w}} \quad [3]$$

where $u^*_{cr-Shields}$ is the theoretical critical shear stress velocity (m s^{-1}).

Critical shear stress velocity calculated from Hjulström curve ($u^*_{cr-Hjulström}$)

Hjulström (1935) presented threshold values for erosion in the unit “current velocity”. His data reflect the effect of cohesion describing a zone of transition between a stable sediment surface and movement of particles. Zanke (1977) gave the following adjustment to the Hjulström plot:

$$u_{cr-Hjulström} = 2.8 (r' g d)^{1/2} + 14.7 \frac{\mathbf{u}}{d} \quad [4]$$

where $u_{cr-Hjulström}$ is the theoretical critical current velocity (m s^{-1} ; see above for definitions of other variables).

Values of $u_{cr-Hjulström}$ had to be transformed into critical shear stress velocities (solid line in Fig. 13, p. 36). For this purpose the quadratic friction law (Eq. [5]) is widely used (e.g. Soulsby 1983, Wright 1989, Poulos 2001). This combines the current velocity u via

a drag coefficient C_D to the shear stress (τ and u^* respectively), assuming a logarithmic velocity profile. This profile is typically developed within the first 1 - 2 m above the bottom (Wright 1989). The drag coefficient varies with the height above bottom and the roughness of the sediment surface (roughness length z_0). A common figure as assumption is $C_D = 0.0025$ as a depth-averaged approximation (Soulsby 1983). When transforming the Hjulström plot, this assumption is suitable, because the velocities given by Hjulström are also depth-averaged values (Zanke 1982).

$$u^*_{cr-Hjulström} = \sqrt{C_D} u_{cr-Hjulström} \quad [5]$$

where $u^*_{cr-Hjulström}$ is the theoretical critical shear stress velocity (m s^{-1}), and C_D the drag coefficient (0.0025 as approximation).

Critical shear stress velocity calculated from flow velocities ($u^*_{cr-flow}$)

At the fine sand station *in situ* flow velocities were measured with an inductive current meter (ISM 2000 – Messen Nord GmbH; effective range of $\pm 3 \text{ m s}^{-1}$, resolution of 1 mm s^{-1} , measurement error of $\pm 3 \text{ cm s}^{-1}$) at 1.5 m above the sea floor. Temperature, salinity, pressure, flow velocity and direction were recorded every hour from July to September and from October to December 2001. Based on current measurements and mean grain sizes, shear stress velocities (u^*_{flow}) at the fine sand station were calculated (see below).

Modelled flow velocities at both investigated sites were obtained from a combination of current and wave energy deriving from a circulation model based on the “Modular Ocean Model” (MOM-2, Pacanowski 1996). Its hydrographic circulation and wave module are forced by an atmospheric module by adopting weather data from the model HIRLAM (Gustafsson 1993). A one-year simulation (Oktober 1996 – September 1997) was used to describe the hydrographic regime in the study area (Rietz et. al. 2000, Bobertz 2001). The vertical resolution varies with water depth. For the data used in this

study, a height of the lowermost model box of 1.5 m above the seafloor was taken for calculations.

The Karman-Prandtl-relationship (e.g. Soulsby 1983, Wright 1989) is applied (Eq. [6]), which relates current velocity $u_{(z)}$, measured at a distinct height z within the logarithmic velocity profile, to shear stress velocity u^* :

$$u_{(z)} = u^* \ln \left(\frac{z}{z_0} \right) \frac{1}{k} \quad [6]$$

where $u_{(z)}$ is current velocity (m s^{-1}) at a height z above the bottom (m), z_0 the roughness length (m), and k the Karmans' constant ($k = 0.4$, e.g. Soulsby 1983). Roughness length, z_0 , does not correspond to the geometric height of microtopographic features, but rather is a length scale representing interaction of these features with the flow. Because hydrodynamic conditions are smooth turbulent (roughness Reynolds number $Re^* = \mathbf{r}_w u^* d (\mu)^{-1} < 3.5$) the widely used approximation for z_0 under rough turbulent conditions ($z_0 = k_s (30)^{-1}$) can not be applied. So, z_0 is determined by a formula from Dade et al. (2001), which is applicable for all values of Reynolds numbers:

$$z_0 = \left[1 - \exp \left(- \frac{u^* k_s}{28u} \right) + \frac{10u}{3u^* k_s} \right] \frac{k_s}{30} \quad [7]$$

where k_s is the effective bed roughness (here, granular roughness), and $k_s = d$ (mean grain size [m], see below).

Under the assumption of a flat bed without any bed forms and a domination of grain size roughness, the effective bed roughness k_s of cohesionless sediments is equal to the mean grain size (e.g. Poulos, 2001) and thus $k_s = d$ in Eq. [7] (granular roughness). Alternative assumptions for k_s can be found in, for example, Soulsby (1997). Dade et al. (2001) pointed out, that in the case of smooth turbulent conditions, k_s has negligible effects on the overlying flow. In this case, the assumption $k_s = d$ may be acceptable for

both sediment types and the effects of sediment preparation for grain size analysis are negligible for the calculation of z_0 .

For the fine sand station with a mean grain size $d = 132 \mu\text{m}$ and a current velocity $u_{(z)}$ at 1.5 m above bottom, the following relationship can be deduced from Eq. [6] and [7]:

$$u^*_{flow} = 0.0445 u_{(150)}^{0.9238} \quad [8]$$

where $u_{(150)}$ is current velocity at 150 cm above the bottom (m s^{-1}).

For the mud station with a mean grain size $d = 21 \mu\text{m}$ the following relationship results from Eq. [6] and [7]:

$$u^*_{flow} = 0.0449 u_{(150)}^{0.9203} \quad [9]$$

Tab. 1: Definitions of calculated and measured shear stress velocities.

Term	Description	Derived from	Author
$u^*_{cr-Shields}$	Calculated from Shields parameter (for cohesionless sediments).	Eq. [2] and [3]	Soulsby and Whitehouse (1997)
$u^*_{cr-Hjulström}$	Calculated from Hjulström curve (including cohesive effects).	Eq. [4] and [5]	Zanke (1977)
$u^*_{cr-initial}$	Initial particle transport	Microcosm device	this study
$u^*_{cr-erosion}$	Particle erosion	Microcosm device	this study
u^*_{flow}	Calculated from measured and modelled flow conditions.	Eq. [8] or [9]	this study

In this context it has to be mentioned that calculations of shear stress velocities at the mud station referred to disaggregated, mainly silt-sized grains. This was due to the pretreatment of sediment samples before analyzing grain sizes (see Bohling 2003 for a detailed description of the method).

Analysis of sediment parameters

After the removal of the 20 cm cores, the remaining sediment surface of the box-corer (~0.07 m²) was sampled with plexiglas cores of 36 mm in diameter. The smaller cores were treated as subsamples of the 20 cm cores in order to describe the properties of the sediment surface used for erosion experiments.

The upper 5 mm of 3 cores were sliced and frozen at -20° C on board for later analysis representing 3 replicate samples per occasion and site. Water content (% of sediment dw) was determined by weighing and drying subsamples to constant weight at 105°C.

Chlorophyll *a* equivalents (*Chl*)

Chlorophyll *a* equivalents (*Chl*) as an indicator of diatom biomass were measured by the acidification method of Holm-Hansen et al. (1965) using 0.5 cm³ of defrosted sediment. *Chl* was extracted in 90% acetone and analysed in a Turner Design Fluorometer (Model 10-AU-005). Calculations of concentrations are based on the JGOFS protocol (UNESCO 1994).

In the presence of chlorophyll *b*, chlorophyll *a* content may be underestimated seriously using the acidification method (e.g. Daemen 1986). To test this hypotheses, sandy sediment samples were taken at 1 m water depth at Warnemünde Beach and frozen at -80° C. Concentrations of *Chl* were measured using reserved phase HPLC (high performance liquid chromatography) and the fluorometric method as described above.

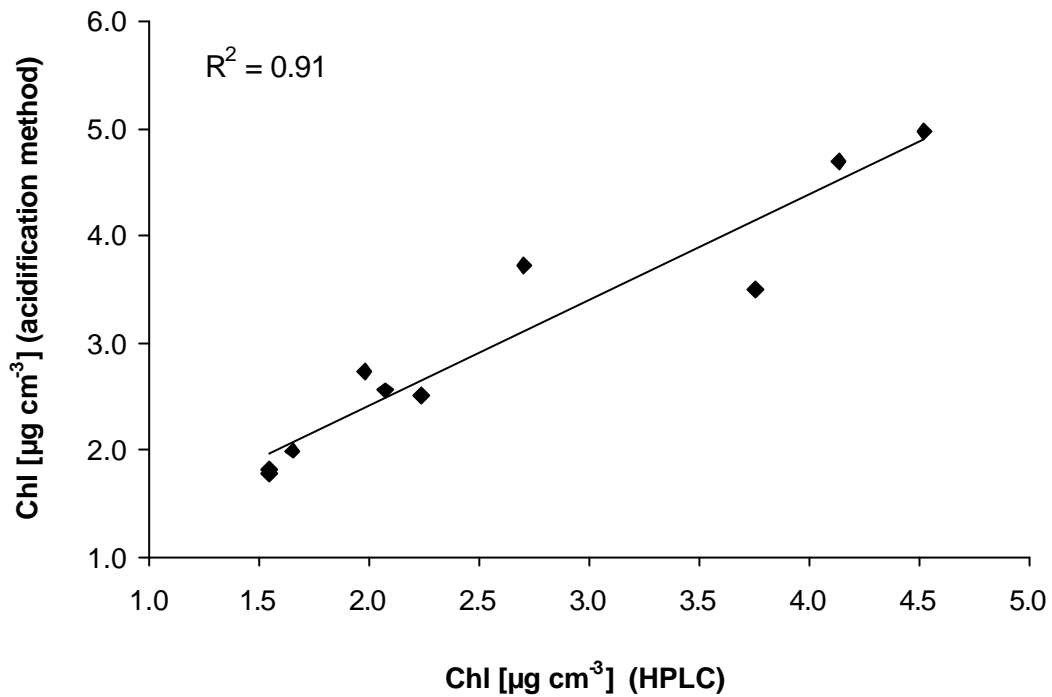


Fig. 7: Correlation between *Chl* measured with HPLC and the acidification method according to Holm-Hansen et al. (1965). Pigments were extracted in 100% acetone from the upper 0 - 1 cm in 1 mm steps of sandy sediments ($n = 10$).

For *Chl* determination with HPLC, pigments were detected by fluorescence emission (excitation wavelength 440 nm, detection wavelength 650 nm) using a Merck-Hitachi fluorescence detector. Results of *Chl* extracted from frozen sediment samples at this site in both -20°C and -80°C revealed comparable results with HPLC (Forster pers. comm.). A significant correlation was assessed between results of *Chl* concentrations in the upper 10 cm of the sediment using the two different methods ($r = 0.95$, $P < 0.01$, $n = 10$, Fig. 7). Thus, values of *Chl* deriving from acidification method predict reasonable results for algal pigment concentrations.

Carbohydrate equivalents (*CHE*)

Colloidal carbohydrate equivalents (*CHE*) were extracted from 100 mg of freeze dried sediment in either 25‰ saline or 100 mM Na₂EDTA (EthylenDiniTrilo etra-acetic Acid) to obtain a water soluble (*Col S*) and water insoluble (*Col EDTA*) fraction. Carbohydrate concentration as an indicator of *EPS* was measured using the phenol-sulfuric acid assay (Underwood et al 1995). The absorbance was measured at 488 nm against a reagent blanc. All results are expressed as glucose equivalents.

Benthic diatom abundance

One 36 mm core per site was taken in July 2001, October 2001 and January 2002 for enumeration of benthic diatom cells. Sediment from the upper 5 mm of each core was sliced and preserved with formaldehyde at a final concentration of 4%. Diatom cells were removed from substrate by ultrasonication (2 min) and counted after using an inverted microscope according to Utermöhl (1958).

Irradiance measurements

A 12 h time series of photosynthetic active radiation (*PAR*, equal quantum response from 400 to 700 nm) was recorded at the mud station in July 2001 (Turnewitsch and Graf 2003) using a calibrated Log Quantum Scalar Irradiance Sensor (QSP-200L; Biospheric Instruments Inc., San Diego) mounted on top of a CTD frame. The sensor had a spin-off value of 0.85 $\mu\text{E m}^{-2} \text{s}^{-1}$. Values of surface irradiance and wind speed during the cruises in July 2001, October 2001 and January 2002 measured from shipboard meteorological measurements were taken every 5 minute. Subsurface irradiance (I_0) was calculated from surface irradiance measurements and reflection of irradiance at the sea surface depending on wind speed and altitude of the sun using the scheme provided by (Walsby 1997).

Depth depending *PAR* was assessed using the exponential light extinction equation:

$$I_z = I_0 e^{-kz} \quad [10]$$

where I_0 is the subsurface irradiance ($\mu\text{E m}^{-2} \text{s}^{-1}$), I_z the irradiance at a water depth (z) and k is the attenuation coefficient. Two different attenuation coefficients (0.2 and 0.5) were used to determine values of *PAR* at the seafloor delineating the prevailing range of k in the investigation area. From *in situ* *PAR* measurements in July 2001, values of $0.2 < k < 0.5$ were determined (Fig. 18, p. 43). This correspond to a mean value of $k = 0.5$ given for Baltic coastal waters (Dera 1995).

Roller table experiments

Experimental setup

In one laboratory experiment, aggregation dynamics of surface particles from coastal sediments were determined (*Exp I*). The influence of added pelagic algae (*Skeletonema costatum*) on aggregation behaviour of the same source of surface particles was measured in a second experiment (*Exp II*). This common diatom species is abundant in the southern Baltic Sea during spring bloom (Wasmund et al. 1998) and shows high stickiness and flocculation behaviour (Kioerboe and Hansen 1993).

Sediment cores with a diameter of 20 cm were taken from an adjacent site of the fine sand station ($54^\circ 12.00' \text{ N}$, $11^\circ 58.00' \text{ E}$, 16 m water depth) in November 2002. Unconsolidated particles from the top layer of the sediment surface were experimentally resuspended from cores with the erosion device microcosm. The lid of the device was removed at critical shear stress velocity for erosion ($u^*_{cr-erosion}$). The water overlying the sediment core containing resuspended particles was immediately collected. To

describe composition of resuspended particles in suspension (SP), subsamples were taken and analysed for different parameters (see below for particle analysis).

For *Exp II*, cultured microorganisms (non-axenic *Skeletonema costatum*) were mixed with particles resuspended from a second core. In both experiments, one litre of the water (SP) was transferred into three replicate cylindrical tanks and filled up with filtered seawater to a final volume of 1.25 dm³ each. The tanks, thus filled with a sediment suspension were placed in a plastic tube equipped with a video camera system (Sony Handycam with close-up lens +4). They were slowly rotated for 18 h on a roller table (Shanks and Edmondson 1989) at a rotation speed of 5 cm s⁻¹ and a temperature of 15° C (Fig. 8).

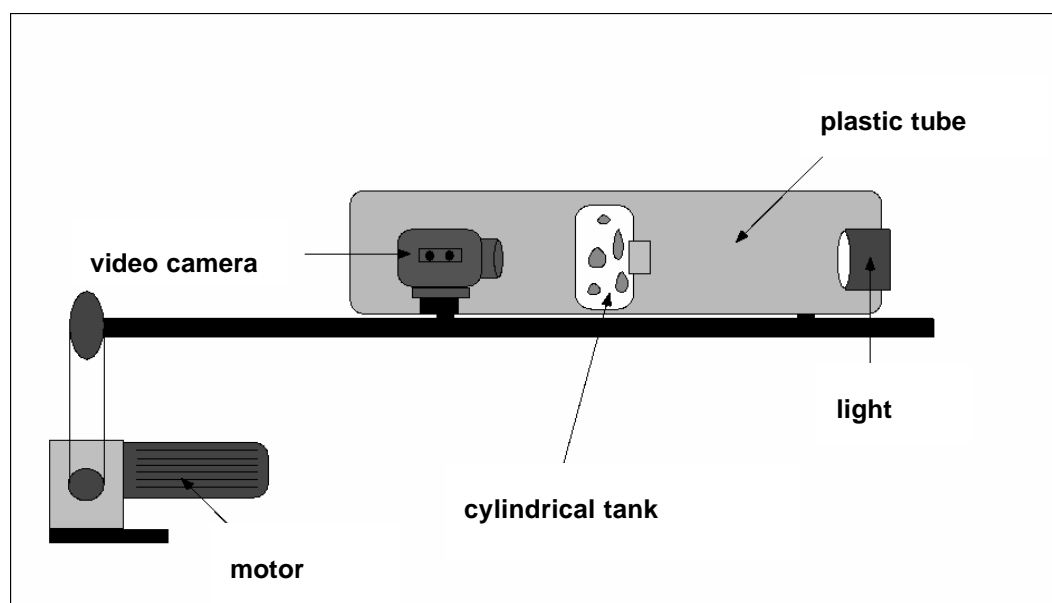


Fig. 8: Schematic view of the experimental setup containing a roller table with the plastic tube and its properties (redrawn after Jähmlich and Graf 1998).

With the camera 10 cm in front of the first tank, particles >100 μm diameter could be identified. During roller table incubation, particle aggregation was recorded every hour for one minute in an area of 3 x 2 cm in size at a radial distance of 3 cm from the centre of the tank (Fig. 9).

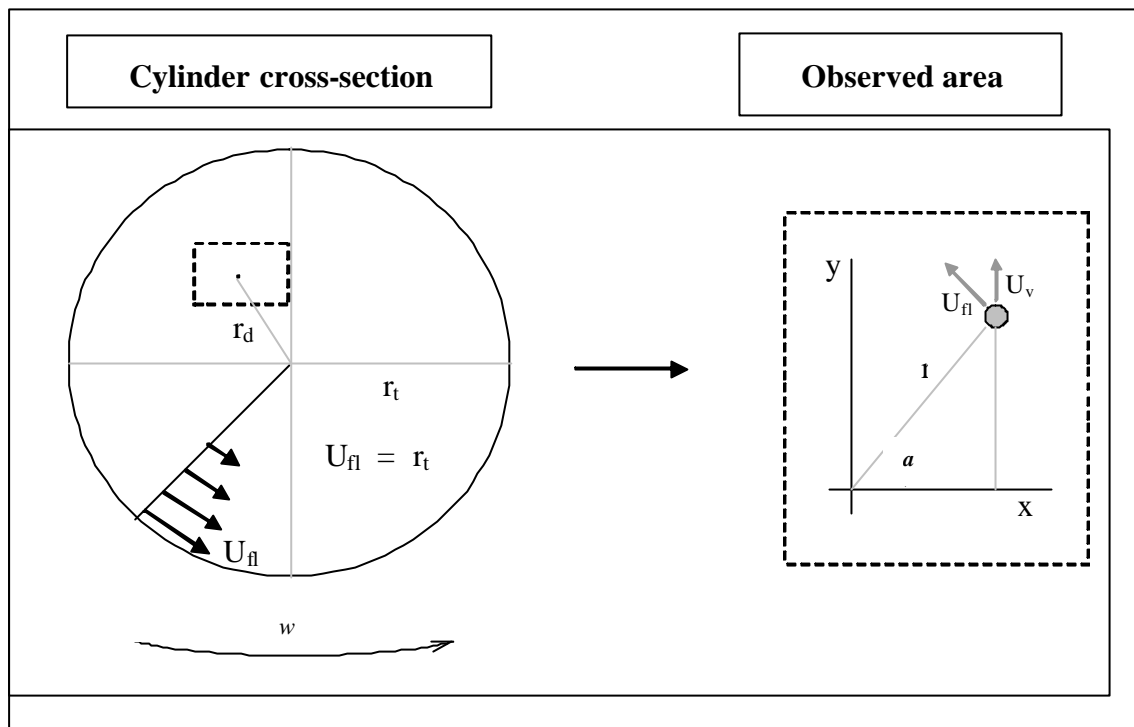


Fig. 9: Scheme of a roller cylinder (left) and the observed area (right), both in cross-section. In the case of solid body rotation, the tangential velocity of the fluid (U_{fl}) is a function of the cylinder radius (r_t) and of the radial velocity (w). Under this condition, the settling velocity (W_{s-cal}) of an aggregate can be calculated from changes in vertical position [Eq. 11]. r_d – radial distance of the observed area from the centre of the tank (3 cm); r_t – cylinder radius (7.5 cm); r – radial distance of an aggregate to left corner of the observed area; U_v – vertical velocity of an aggregate in the x-y plane, given by $U_v = w r \cos a$ (redrawn after Engel and Schartau 1999).

Video pictures were digitised on a Macintosh computer and analysed with the software “Image 1.4”. At each time interval the largest diameter of between 17 and 58 sharp edged aggregates was measured to determine mean particle diameter growth rates of aggregates forming in the tank. Furthermore, the following parameters of aggregates were measured to calculate settling velocities (W_{s-cal} , Eq. 11) according to Engel and Schartau (1999): visible velocity (AU_A) of an aggregate in the video picture, length of the major and minor axis, largest expansion in the horizontal and vertical direction, position in the x-y plane. The determination of the latter parameter consisted of the following procedures: First, the aggregate position in the video picture was measured

with image analysis on a micrometer scale and second, the position of the aggregate in the x-y plane of the tank was calculated as the radial distance of the video picture to the centre of the tank (millimetre scale).

At the end of each roller table experiment, the tanks were carefully turned to one side and aggregates were allowed to settle to the bottom. The overlying water (W) above the settled macroscopic aggregates was sampled and analysed for different parameters (see below).

Small aggregates invisible for the naked eye were certainly present in W . Individual large aggregates were removed from the tanks using a syringe and transferred to a glass cylinder with a volume of 2 dm³. Sinking particles were recorded with the same video camera as described above to determine settling velocities (W_{s-exp}) with “Image 1.4”. Aggregates were collected in a petri dish at the bottom of the cylinder and combined with the original water containing aggregates left over in the tank ($W+A$). This material was filtered and analysed for different parameters as well.

Thus, water samples were taken before (SP) and after each roller table experiments (W and $W+A$). Concentrations of parameters for aggregates formed during roller table experiments (A) were calculated from W and $W+A$ and values are given in table 2.

Sinking velocity of aggregates during solid body rotation in the tank was independently derived from its visible velocity (AU_A):

$$W_{s-cal} = U_v + AU_A \quad (11)$$

where U_v is the vertical component of the fluid velocity (Fig. 9). Detailed geometrical considerations of the cylindrical tanks are given in (Engel and Schartau 1999).

Water samples

Total suspended particulate matter (*SPM*)

Water samples of 50 and 100 cm³ in volume were filtered and analysed for different parameters to complement the results from image analysis.

Total suspended particulate matter (*SPM*) was measured according to von Bodungen et al. (1991) using pre-weighed glass fibre filters (0.7 µm pore size). Samples were filtered and frozen at -20° C. Before reweighing, filters were oven dried. The analytic precision of reweighing filters can be within ± 10% (von Bodungen et al. 1991).

Chlorophyll *a* equivalents (*Chl*)

Chlorophyll *a* equivalents (*Chl*) were filtered onto glass fibre filters (0.7 µm pore size), extracted in 90% acetone and measured by the acidification method as described above (see p. 22).

Particulate organic carbon and nitrogen (*POC* and *PON*)

Particulate organic carbon (*POC*) and particulate organic nitrogen (*PON*) were measured using a EA 1110 element analyser (CE Instruments) in continuous flow mode. Prior to the measurements, filters were acidified to remove inorganic carbon. Acetanilide standards were used for calibration. The analytic precision can be within ± 4% (von Bodungen et al. 1991). Concentrations of *POC* and *PON* were calculated according to the JGOFS protocol (UNESCO 1994).

Biogenic sticky particles (*CHE* and *TEP*)

Carbohydrate equivalents (*CHE*) were determined using the phenol-sulfuric acid assay (Underwood et al 1995). Particles were filtered onto glass fibre filters and extracted with distilled water. This extraction procedure is used for the determination of total carbohydrate concentration and differs from extraction procedure of colloidal carbohydrates (see p. 24). Here, all carbohydrates within the range of the assay, including intra- and extracellular, and particle-bound detrital material are hydrolysed and measured. Values are expressed as glucose equivalents used to measure a standard calibration curve.

Beside *CHE*, transparent exopolymer particles (*TEP*) were analysed both indicating biogenic sticky particles in the tanks. These gel-like particles formed abiotically from dissolved excretion products of phyto- and bacterioplankton, were determined according to Passow and Alldredge (1995 b). 20 cm³ of water preserved in formaldehyde at a final concentration of 4% were filtered onto 0.4 µm Nucleopore filter and stained with Alcian blue. Concentrations of *TEP* are expressed as gum xanthan equivalents used to measure a standard calibration curve (Fig. 10).

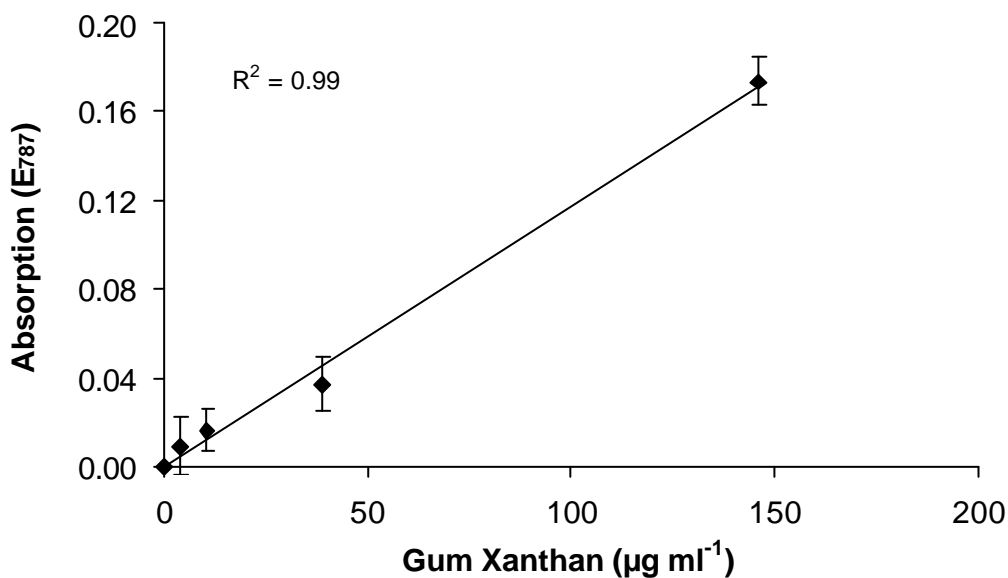


Fig. 10: Calibration curve made with a gum xanthan solution for the used batch of alcian blue (mean values \pm s. d., $n = 4$).

The calibration standard was prepared by mixing ~15 mg of gum xanthan into 200 ml of distilled water resulting in a viscous solution including gel-like particles. In order to determine the weight of gum xanthan particles retained on a 0.4 μm filter, 1.5 ml of the standard solution was filtered onto preweighed Nucleopore filters. The dry weight was used to calculate the calibration factor according to Passow and Alldredge (1995 b).

Bacteria and diatom abundance

For the determination of bacterial abundance, 10 cm^3 water samples were preserved with formaldehyde at a final concentration of 4%. Bacteria were stained with DAPI (4', 6-DiAmidino-2-PhenylIndol) and enumerated by epifluorescence microscopy according to Porter and Feig (1980).

Diatom cells were counted using an inverted microscope according to Utermöhl (1958) from 20 cm^3 of water fixed with formaldehyde at a final concentration of 4%. Cultured cells of the genus *Skeletonema* and pennate benthic diatoms, resuspended from the sediment surface during microcosm experiments, were distinguished.

Statistical analysis

All biochemical data from sediment and water analysis were assumed to be normally distributed. This was tested for sediment samples taking 13 plexiglas cores of 36 mm diameter from one box-corer at the fine sand station in September 2000.

Sediment cores were treated as described above and *Chl* was measured in the upper 5 mm of each core according to Holm-Hansen et al. (1965). Values of *Chl* given in figure 11 were normally distributed about the mean value of $5.2 \pm 1.3 \text{ mg m}^{-2}$ ($P < 0.05$). This result justifies the use of three replicate cores for the determination of sediment parameters predicting representative results for parameters in the investigated sediment area. Although, patchiness effects of sediment properties on the area of the box-corer could not be excluded (see p. 57).

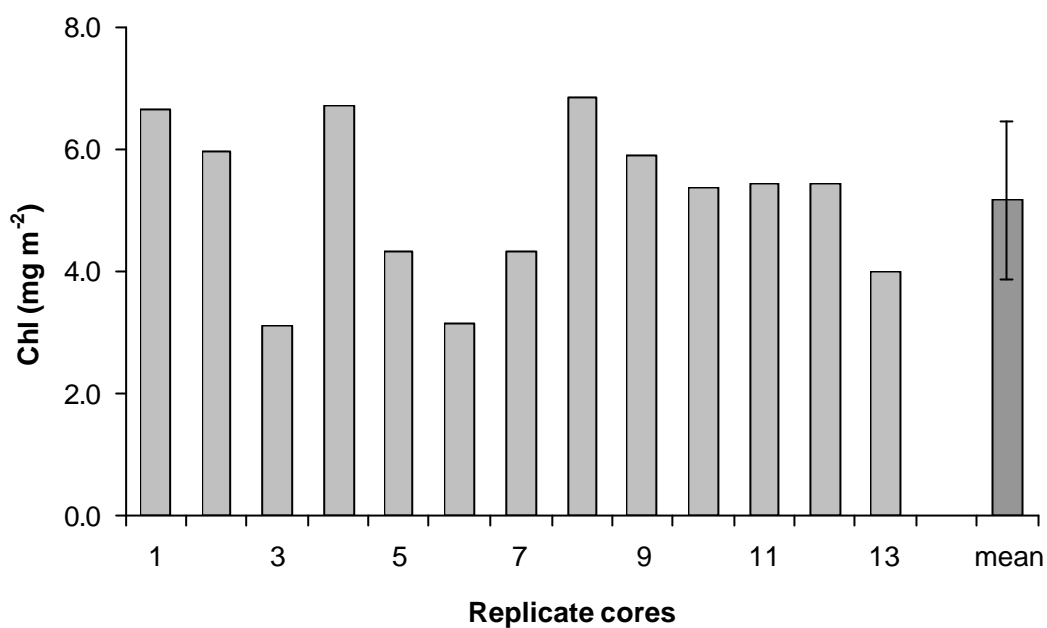


Fig. 11: Concentrations of *Chl* in the upper 5 mm of replicate cores ($n = 13$, mean \pm s.d.) taken in one box-corer at the fine sand site in September 2000. Values were tested being normally distributed about the mean value ($P < 0.05$).

Pearson's correlation coefficients were calculated to examine relationships between measured parameters. The values of significance were calculated using a *t*-test. Differences between values of sediment parameter were examined using an analysis of variance (one-way ANOVA) at a 5% significance level.

Results

Erosion experiments

Mud cores

Sediment surfaces at the mud station were covered by a homogenous, fluffy layer at each sampling occasion. The thickness of fluff varied between a few millimetres in January 2002 and about 1 cm in September 2000. Differences in erosion behaviour of duplicate cores were tested in January 2002 and are negligible (blue lines in the upper graph of Fig. 12).

Values for $u^*_{cr-erosion}$ for mud varied between 0.4 and 0.6 cm s⁻¹, except for July 2001. Here, $u^*_{cr-erosion}$ increased to 1.0 cm s⁻¹ exceeding the threshold value of 0.75 cm s⁻¹ for sieved mud (dotted line in the upper graph of Fig. 12). All in all, thresholds of $u^*_{cr-erosion}$ varied by a factor 2 at this location.

The threshold for initial particle transport showed a variation of a factor 1.6 during the sampling period, with the highest value in July 2001 (0.5 cm s⁻¹). A significant positive relationship between both thresholds exists ($r = 0.83$, $P < 0.1$, $n = 5$, Tab. 2).

Fine sand cores

At the fine sand station sediment surfaces were more heterogeneous compared to mud sediments because of sediment ripples and biogenic structures (mussel shells and worm tubes). Still, variations in erosion behaviour remained low among replicate cores in September 2000 and January 2002 (green and blue lines in the lower graph of Fig. 12).

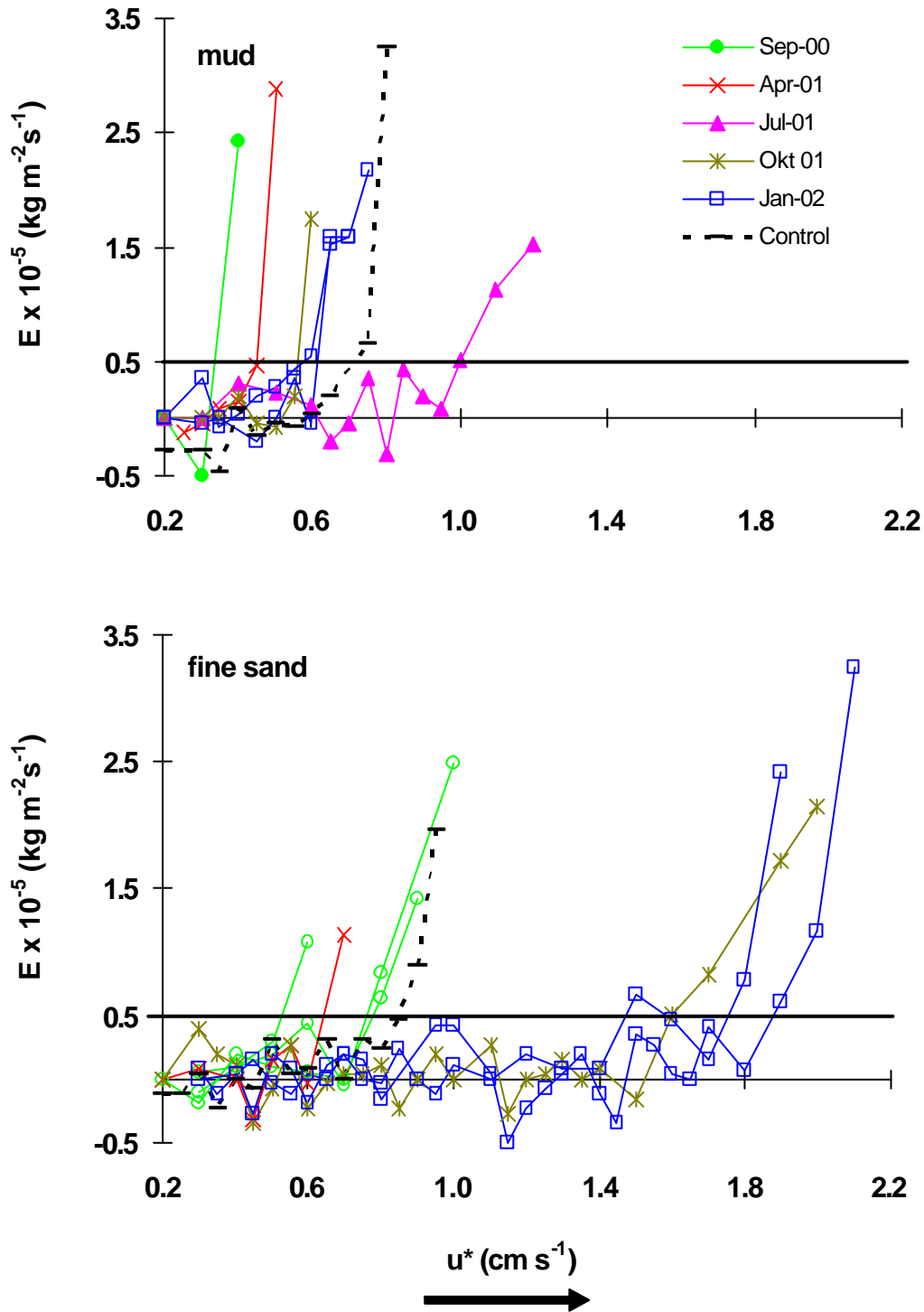


Fig. 12: Erosion flux (E) from mud (upper graph) and fine sand cores (lower graph) at different sampling dates. Negative values of E may indicate particle deposition during erosion experiments (see section of Materials and methods for calculation of E). Dotted lines indicate erosion of control cores with sieved mud and fine sand sediment. Horizontal lines stand for the threshold of $u^*_{cr-erosion}$ ($0.5 \times 10^{-5} \text{ kg m}^{-2} \text{ s}^{-1}$).

The lowest value for $u^*_{cr-erosion}$ was 0.7 cm s^{-1} measured in September 2000 (mean value of $n = 3$) and April 2001. In October 2001 and January 2002 (mean value of $n = 2$ cores) the highest value of $u^*_{cr-erosion}$ of 1.7 cm s^{-1} was measured exceeding the threshold value of 0.9 cm s^{-1} for sieved fine sand sediment (dotted line in the lower graph of Fig. 12). Thus, during sampling period $u^*_{cr-erosion}$ varied by a factor 2.4.

In September 2000 and April 2001, initial particle transport was detected at 0.4 and 0.35 cm s^{-1} , respectively. Values for $u^*_{cr-initial}$ increased to 0.55 and 0.6 cm s^{-1} in October 2001 and January 2002 compared to former sampling dates (factor 1.7). A positive significant correlations was found between $u^*_{cr-initial}$ and $u^*_{cr-erosion}$ ($r = 0.97$, $P < 0.05$, $n = 4$, Tab. 2).

At the mud station net erosion flux (E) corresponding to $u^*_{cr-erosion}$ tended to be higher up to a factor 2.5 compared to the fine sand station. A significant negative relationship between E and $u^*_{cr-erosion}$ was found at both the mud ($r = -0.74$, $P < 0.1$, $n = 6$) and the fine sand station ($r = -0.76$, $P < 0.05$, $n = 7$).

Erosion thresholds compared to calculated u^* values

Figure 13 illustrates resuspension curves based on the Shields parameter and the Hjulström plot. Experimentally derived threshold values were integrated in this figure, although, mean grain size of both stations do not refer to particle sizes of resuspended material but to sediment samples from the upper 5 cm including disaggregated surface particles.

Mean values of $u^*_{cr-initial}$ from both sediment types were comparable and did not exceed calculated thresholds. Erosion thresholds of mud ($u^*_{cr-erosion}$) were less than calculated values except for July 2001. Although the mean value of $u^*_{cr-erosion}$ (0.6 cm s^{-1}) fits well with the results of Soulsby and Whitehouse (1997), $u^*_{cr-Shields} = 0.8 \text{ cm s}^{-1}$ [Eq. 3], it is roughly 6 times smaller than the calculated values in the Hjulström plot for cohesive mud ($u^*_{cr-Hjulström} = 3.75 \text{ cm s}^{-1}$, [Eq. 4]).

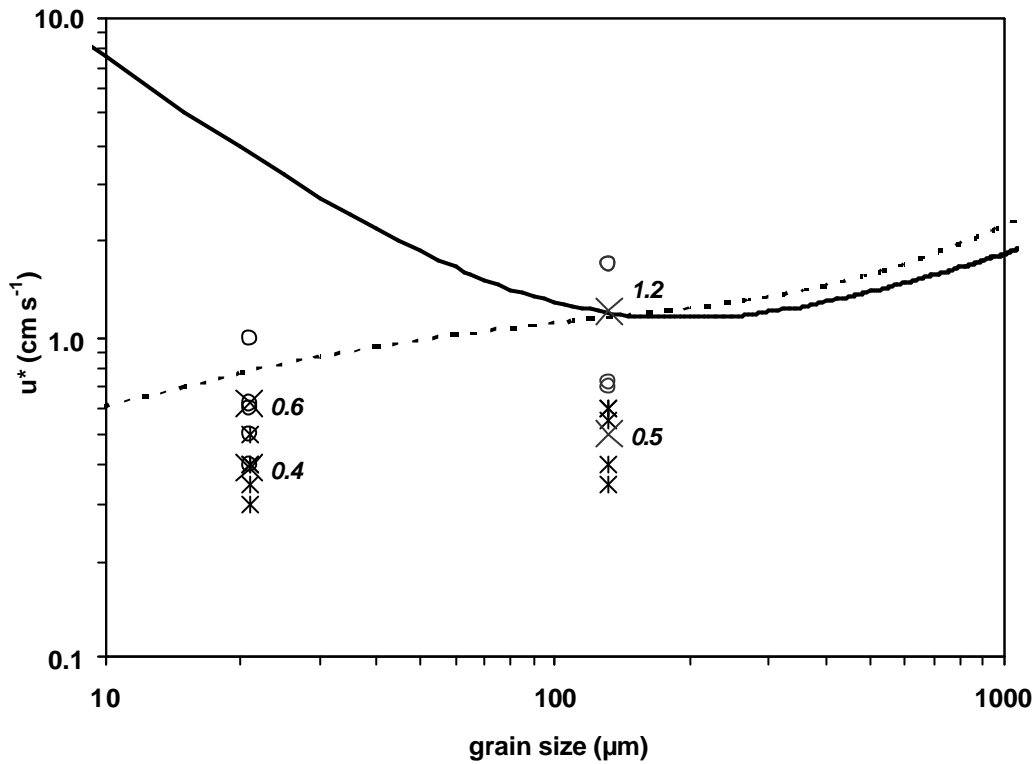


Fig. 13: Resuspension curves based on Shields parameter (dotted line) and Hjulström plot (solid line; see Materials and methods for calculations) and erosion thresholds measured on single cores of both sites with \circ : $u^*_{cr-erosion}$ and \times : $u^*_{cr-initial}$. Numbers represent mean values of experimental critical shear stress velocities (\times) calculated from results of single cores (lower values: mean $u^*_{cr-initial}$; higher values: mean $u^*_{cr-erosion}$). Mean grain sizes of both sediment types refer to the upper 5 cm of sediment surfaces.

The value of mean $u^*_{cr-erosion}$ at the fine sand station (1.2 cm s^{-1}) is equal to the estimate of the Hjulström plot and the critical shear stress velocity based on Shields parameter ($u^*_{cr-Hjulström}$ and $u^*_{cr-Shields} = 1.2 \text{ cm s}^{-1}$). However, highest values of $u^*_{cr-erosion}$ determined in October 2001 and January 2002 exceeded both calculated thresholds.

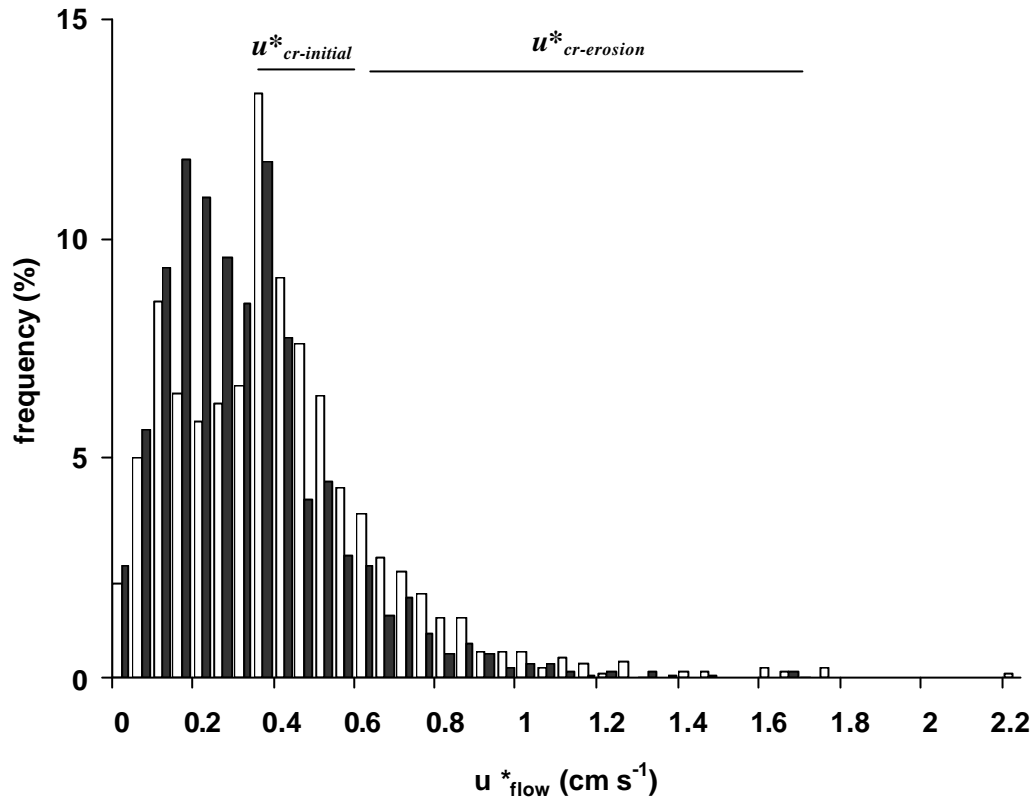


Fig. 14: Frequency distribution of shear stress velocities at the fine sand station (open bars – July to September 2001, $n = 1710$; closed bars – October to December 2001, $n = 1242$). Flow velocities measured with an inductive current meter were transformed into shear stress velocities (see Materials and methods for calculation). Ranges of both measured erosion thresholds at this site are given in the upper part of the graph.

Calculated values of u^*_{flow} deriving from *in situ* flow velocities at the fine sand station (see Eq. 8, p. 21) are presented in figure 14. From July to September 2001, 89% of u^*_{flow} values did not exceed the mean $u^*_{cr-initial}$ of 0.5 cm s^{-1} . The median u^*_{flow} value of 0.26 cm s^{-1} was smaller than the lower limit of $u^*_{cr-initial}$ (0.35 cm s^{-1}). During this period of 3 months, two storm events with values of u^*_{flow} greater than the measured $u^*_{cr-erosion}$ were detected.

From October to December 2001, values of u^*_{flow} were not high enough to reach mean $u^*_{cr-erosion}$ of 1.2 cm s^{-1} . A small amount of high flow events exceeded the lower limit of

$u^*_{cr-erosion}$ (0.73 cm s^{-1}). The median u^*_{flow} value was 0.20 cm s^{-1} . Here, 93% of the u^*_{flow} values were smaller than mean $u^*_{cr-initial}$ of 0.5 cm s^{-1} .

During the one-year simulation of current velocities at the fine sand station (MOM-2, Pacanowski 1996), only one event of u^*_{flow} greater than 1.2 cm s^{-1} was recorded. Most of the values (93%) were less than measured values of $u^*_{cr-initial}$.

At the mud station, 87% of u^*_{flow} values derived from the model were less than the mean $u^*_{cr-initial}$ of 0.4 cm s^{-1} . Considering the threshold for erosion, 90% of the values did not exceed the mean $u^*_{cr-erosion}$ of 0.6 cm s^{-1} . All in all, 39 high flow events with current velocities high enough to reach critical shear stress velocity for erosion were detected.

Sediment parameter

Col S, Col EDTA, Chl

At the mud station, mean concentrations of water soluble carbohydrates (*Col S*) were significantly different from one another (upper graph Fig. 15, $F_{3,48} = 28.32$, $P < 0.001$). The highest *Col S* value of 3.4 g m^{-2} was measured in July 2001 whereas the lowest value of 0.4 g m^{-2} was measured in September 2000. No significant differences were found comparing mean values of water insoluble carbohydrates (*Col EDTA*) ranging between 0.8 and 1.5 g m^{-2} ($F_{3,48} = 1.12$, $P = 0.4$).

At the fine sand station mean values of *Col S* exceeded those from the mud station except for July 2001 (lower graph in Fig. 15). *Col S* concentrations were significantly different from one another ($F_{3,48} = 17.57$, $P < 0.001$) and from values at the mud station ($F_{2,4} = 22.73$, $P < 0.001$) ranging between 0.2 g m^{-2} in July 2001 and 10.5 g m^{-2} in January 2002. Concentrations of *Col EDTA* were significantly different from one another ($F_{3,48} = 4.21$, $P = 0.03$) and from values at the mud station ($F_{2,4} = 32.5$, $P < 0.001$) varying between 0.01 and 0.4 g m^{-2} . Highest values were measured in July 2001.

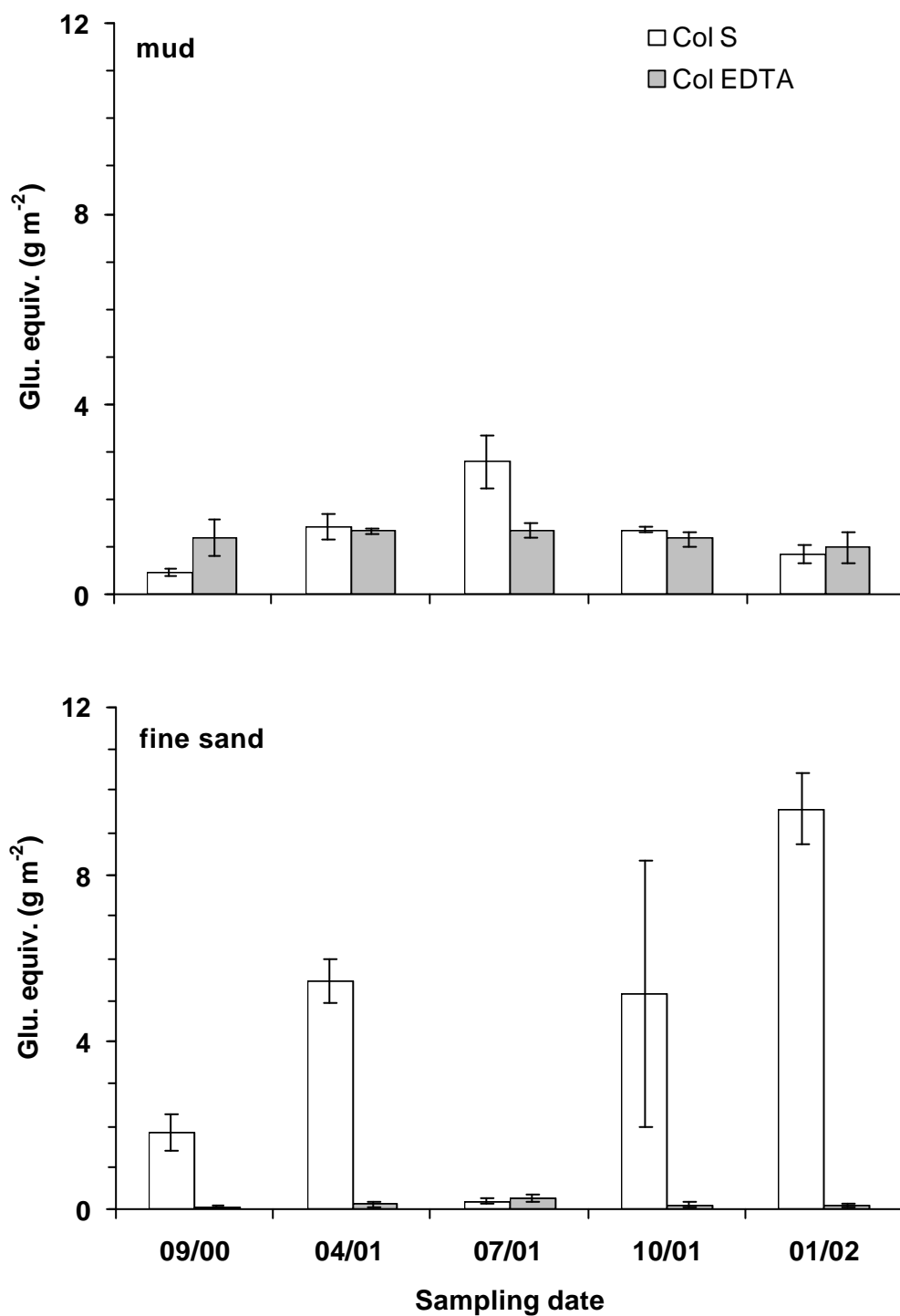


Fig. 15: Mean concentrations with standard deviations ($n = 3$) of colloidal carbohydrates expressed as glucose equivalents in the upper 5 mm of the mud (upper graph) and the fine sand station (lower graph) at different sampling dates. *Col S* – water soluble carbohydrates, *Col EDTA* – water insoluble carbohydrates.

Concentrations of *Chl* at the mud station ranged between 0.7 mg m^{-2} in September 2000 and 7.3 mg m^{-2} in April 2001 being significantly different from one another ($F_{3,48} = 383.3$, $P < 0.001$, Fig. 15). At the fine sand station concentrations of *Chl* varying significantly from one another ($F_{3,48} = 250.6$, $P < 0.001$) were higher compared to the mud station. Values ranged between 4.2 mg m^{-2} in September 2000 and 27 mg m^{-2} in April 2001.

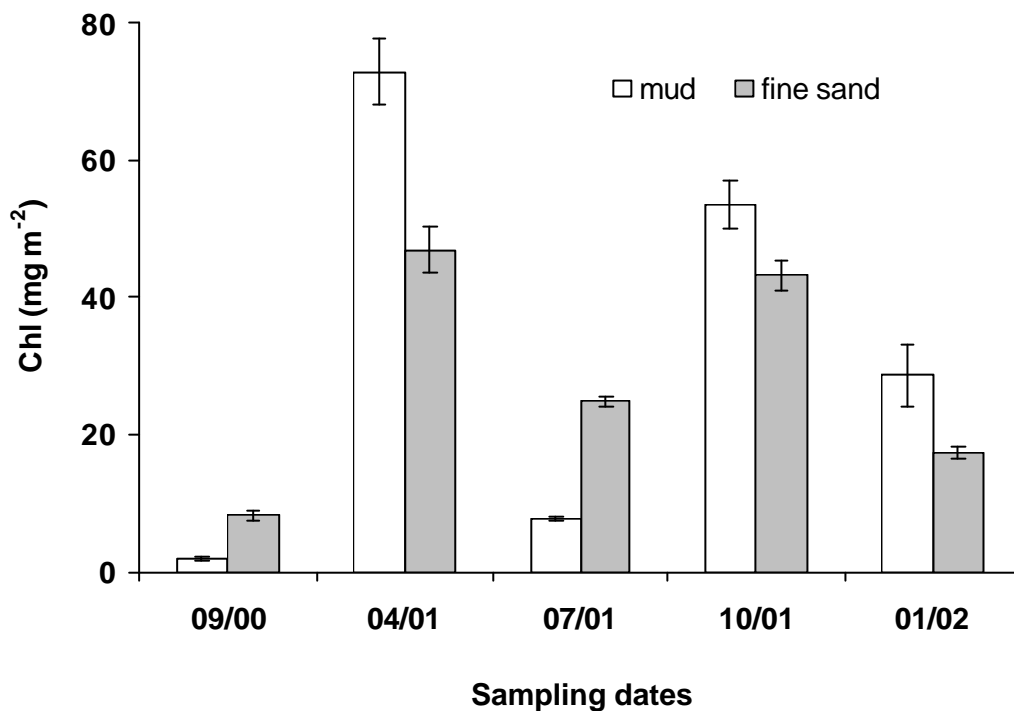


Fig. 16: Mean concentrations with standard deviations ($n = 3$) of chlorophyll *a* equivalents (*Chl*) in the upper 5 mm of mud and fine sand cores at different sampling dates.

Diatom abundances

Samples to determine diatom abundances were taken in July 2001, October 2001 and January 2002 (Fig. 17). Cell numbers at both stations ranged between 5 and $8 \times 10^5 \text{ m}^{-2}$ in July and October 2001 with slightly higher values at the shallower occasion. In January 2002, diatom abundances increased to $26 \times 10^5 \text{ cm}^{-2}$ at the fine sand station and $34 \times 10^5 \text{ cm}^{-2}$ at the mud station. At this sampling date maximum values were found at

the deeper compared to the shallower occasion. All in all, cell numbers increased from July and October 2001 to January 2002 by a factor 4 at the fine sand station and a factor 7 at the mud station, respectively.

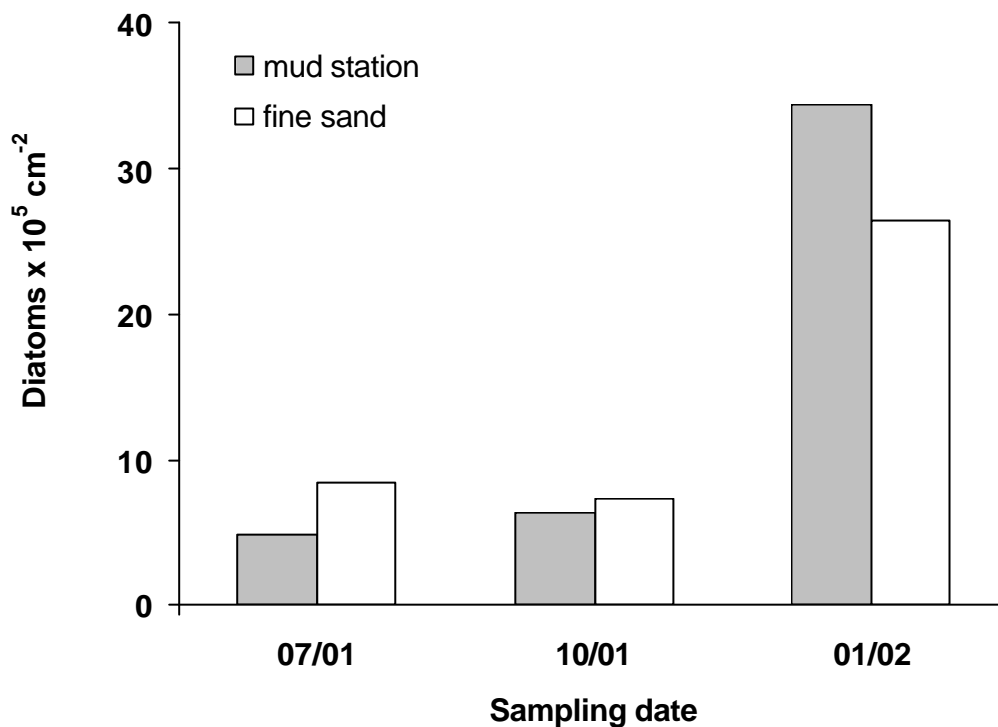


Fig. 17: Cell numbers of pennate diatoms in the upper 5 mm of single mud and fine sand cores at three different sampling dates.

Correlation of sediment parameter and erosion thresholds

Pearson's correlation coefficients were calculated relating mean concentrations of sediment parameter indicative for benthic microorganism biomass (*Chl*) and microbial exudates (*Col S*, *Col EDTA*) with erosion thresholds ($u_{cr-initial}^*$, $u_{cr-erosion}^*$; Tab. 2). Numbers of diatom cells were not included in the correlations because results of abundances were only available from three sampling dates.

Tab. 2: Pearson's correlation coefficients between erosion thresholds and mean values of different parameter in the top 5 mm from the fine sand and mud station ($n = 5$; $n = 4$)^a. $u^*_{cr-initial}$ – critical shear stress velocity for initial rolling transport, $u^*_{cr-erosion}$ – critical shear stress velocity for particle entrainment (see section of Materials and methods for definitions), *Col S* – carbohydrate fraction extracted with saline, *Col EDTA* – carbohydrate fraction extracted with EDTA, *Chl* – Chlorophyll *a* equivalents.

Mud	$u^*_{cr-initial}$ (cm s^{-1})	$u^*_{cr-erosion}$ (cm s^{-1})	<i>Col-S</i> (mg m^{-2})	<i>Col-EDTA</i> (mg m^{-2})	<i>Chl</i> (mg m^{-2})
$u^*_{cr-erosion}$ (cm s^{-1})	0.83*				
<i>Col S</i> (mg m^{-2})	0.99***	0.88**			
<i>Col EDTA</i> (mg m^{-2})	0.63	0.35	0.66		
<i>Chl</i> (mg m^{-2})	0.57	0.10	0.53	0.78	
Water content (% dw)	-0.95**	-0.87**	-0.97***	-0.66	-0.58
Finesand					
$u^*_{cr-erosion}$ (cm s^{-1})	0.97**				
<i>Col S</i> (mg m^{-2})	0.14	0.67			
<i>Col EDTA</i> (mg m^{-2})	0.41	0.00	-0.52		
<i>Chl</i> (mg m^{-2})	-0.17	0.03	0.09	0.27	
Water content (% dw)	0.15	0.48	-0.84*	0.50	-0.55

^a Values of r are significant at: *** = $P < 0.01$, ** = $P < 0.05$, * = $P < 0.1$

At the mud station *Col S* was significantly positive correlated with both erosion thresholds. A significant negative relationship was found between *Col S* and water content. Both erosion thresholds were negatively correlated with water content.

Mean values of *Chl* and *Col EDTA* did not correlate significantly with any of the remaining parameters, although, both parameter showed a positive but no significant relationship with each other and $u^*_{cr-initial}$.

At the fine sand station, too, mean concentration of *Col S* and sediment water content were found to be significantly negative correlated. *Col S* and $u^*_{cr-erosion}$ showed a positive but no significant relationship. All in all, erosion thresholds were not significantly correlated to any of the analysed parameters.

Irradiance measurements (*PAR*)

Measurements of *PAR* were conducted from 2.45 h to 13 h (UTC) at the mud station.

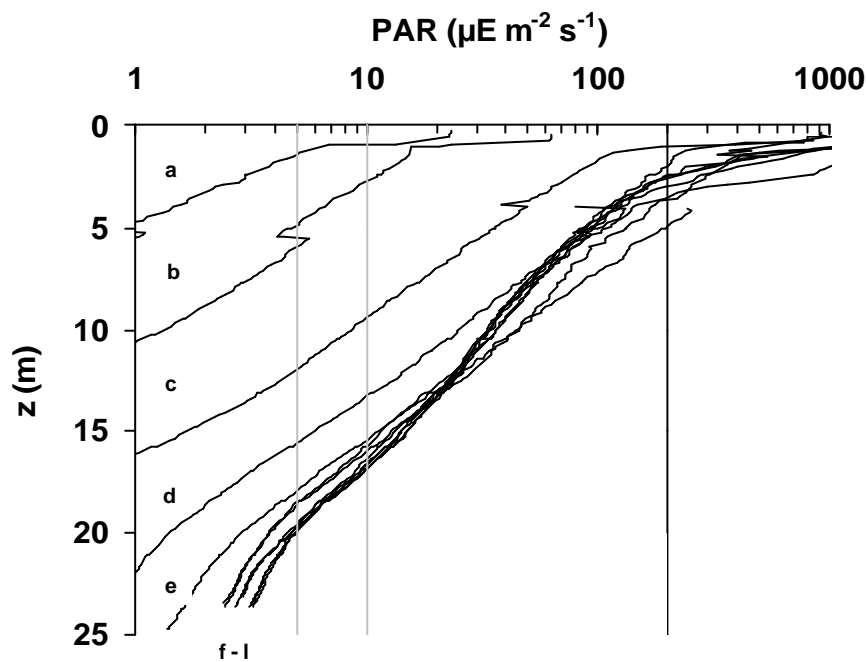


Fig. 18: Vertical profiles of photosynthetic active radiation (*PAR*) in the water column of the mud station in July 2001. a – 2:45 h, b – 3:00 h, c – 4:00 h, d – 5:00 h, e – 6:00 h, f – 9.30 h, g – 10:00 h, h – 10.30 h, i – 11.30 h, j – 12.00, k – 12.30 h, l – 13:00 h (h in UTC). The transparent box indicates lower limit of light intensities ($5\text{-}10 \mu\text{E m}^{-2} \text{s}^{-1}$) for benthic microalgae growth given by (Cahoon 1999). Vertical line stands for the light intensity at which micro-biostabilisation has been measured on subtidal sediments (Madsen et al 1993).

Results revealed an exponential decrease from surface waters to the bottom of the water column with highest values around midday (Fig. 18). However, *PAR* did not reach $5 \mu\text{E m}^{-2} \text{ s}^{-1}$ at water depths exceeding 20 m over the entire measurement period in July 2001.

During midday, this value was passed for approximately 4 hours at depths equal to the fine sand station. Calculated attenuation coefficient (k) varied between 0.2 and 0.5. The weather condition at the sampling day was calm and sunny (hPa = 1015) considering optimal illumination.

Aggregate formation and sinking behaviour of resuspended particles

Aggregate formation

Figure 19 shows mean particle diameters and distribution of particles in size classes formed in roller table experiment I (*Exp I*). Aggregate formation can be separated into a growth phase and a stationary phase. Within the first six hours the relationship between mean aggregate diameter and incubation time was found to be positive significant ($r = 0.93$, $P < 0.01$). During this period, aggregates had a mean diameter growth rate of $260 \mu\text{m h}^{-1}$. After six hours rotation time, mean aggregate diameters remained constant. From that time on, the distribution of particles in size classes was uniform with a slight tendency towards the smallest class during incubation time (lower graph in Fig. 19). Aggregates reached highest values of $5321 \mu\text{m}$ in diameter.

S. costatum aggregates (*Exp II*) showed a continuous mean diameter growth rate of $100 \mu\text{m h}^{-1}$ over 18 hours rotation time with a positive significant relationship between mean aggregate diameter and incubation time ($r = 0.94$, $P < 0.001$, upper graph in Fig. 20). Towards the end of the experiment size class distribution reveal that $>60\%$ of aggregates had diameters exceeding $2000 \mu\text{m}$ with maximum diameters of $6913 \mu\text{m}$ (lower graph in Fig. 20).

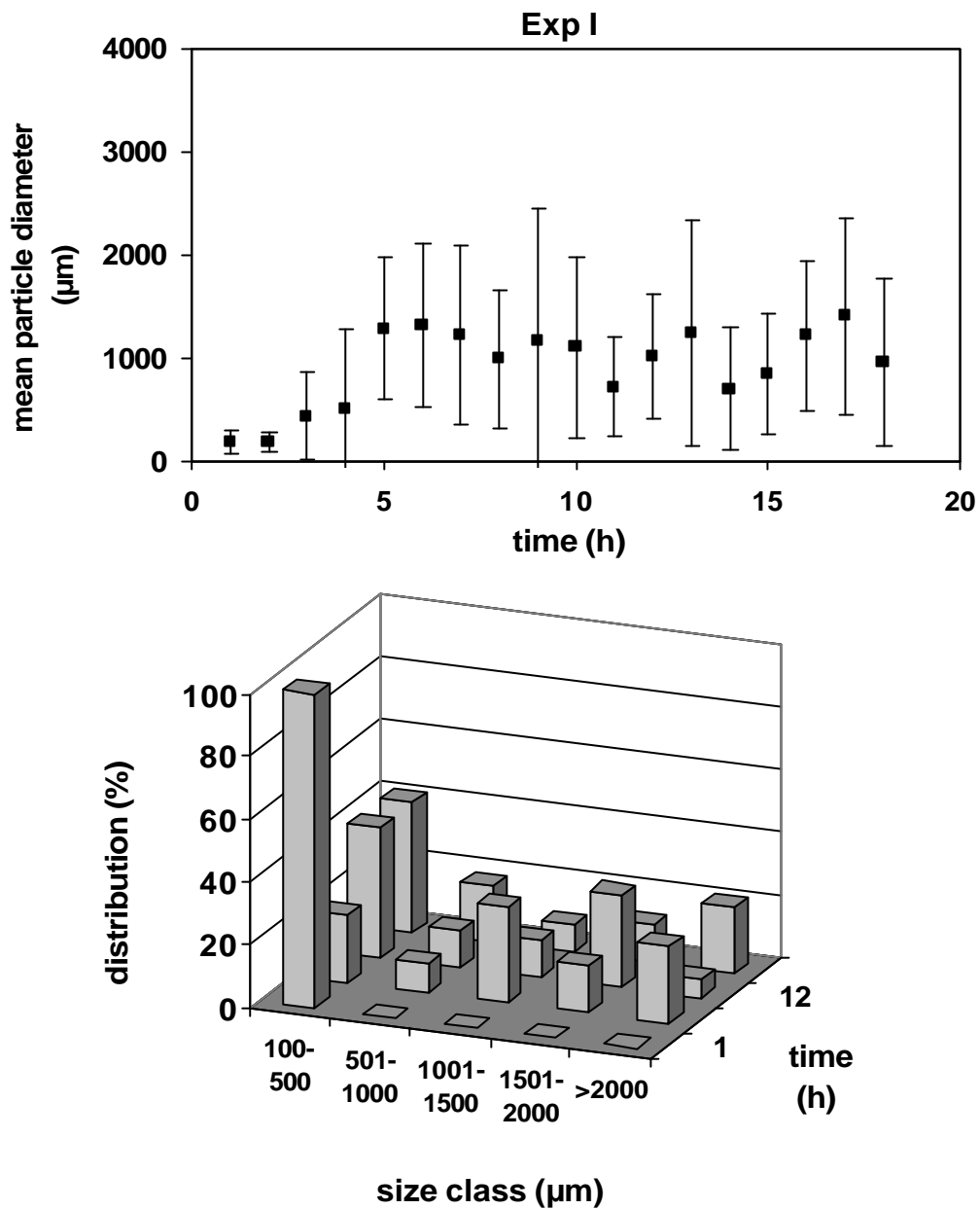


Fig. 19: Mean particle diameter \pm standard deviation during roller table incubation of *Exp I* ($n = 17 - 41$) derived from image analysis (upper graph). No relationship was found between mean particle diameter and incubation time except for the first 6 hours ($r = 0.93$, $P < 0.01$, $n = 6$). Distribution of particles in size classes at four representative times are illustrated in the lower graph.

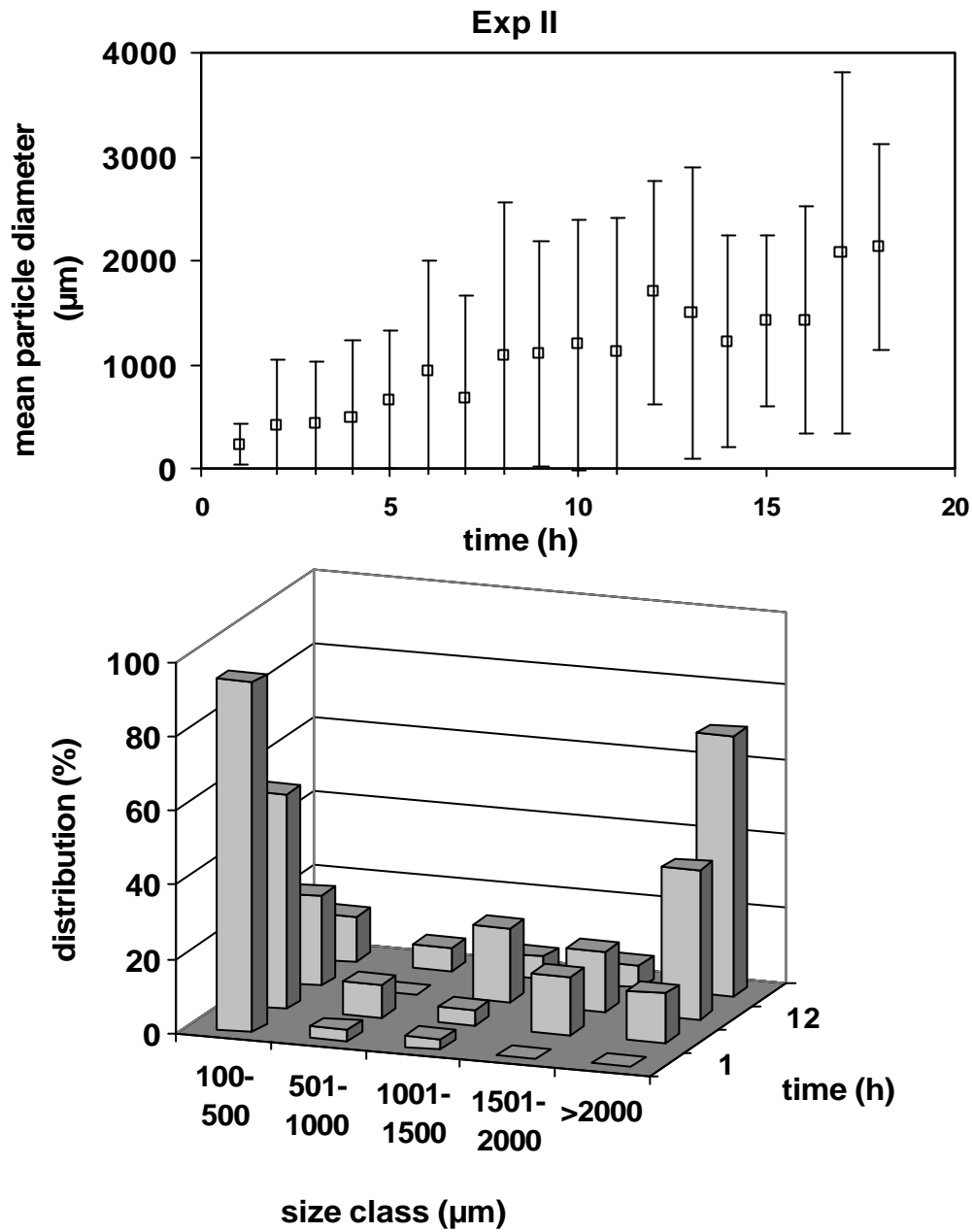


Fig. 20: Mean particle diameter \pm standard deviation during roller table incubation of *Exp II* ($n = 25 - 58$) derived from image analysis (upper graph). A significant linear relationship was found for both parameters in experiment II ($r = 0.94$, $P < 0.001$, $n = 18$). Distribution of particles in size classes at four representative times are illustrated in the lower graph.

Sinking velocities

Settling chamber (W_{s-exp})

Experimentally derived settling velocities ranged from 0.06 to 1.0 cm s⁻¹ for particles formed in both roller table experiments with diameters of 136 to 4416 µm (Fig. 21). In *Exp I*, values of W_{s-exp} did not significantly correlate with particle diameter whereas W_{s-exp} of *S. costatum* aggregates and particle diameter showed a significant positive relationship ($r = 0.84$, $P < 0.001$, $n = 33$). Two size classes were distinguished, varying from <1000 µm to >1000 - 2350 µm in diameter. This classification is based on *in situ* observations revealing that the dominant aggregate sizes in bottom waters of Mecklenburg Bight and an adjacent area are presumably less than 1000 µm (Christiansen et al 2002, Jähmlich et al 1999, Jähmlich et al 2002). Mean aggregate settling velocities in *Exp I* were from 0.2 ± 0.08 cm s⁻¹ for aggregates <1000 µm to 0.3 ± 0.12 cm s⁻¹ for those >1000 - 2350 µm. *S. costatum* aggregates <1000 µm showed mean sinking velocities comparable to aggregates of the same size class formed in *Exp I*, while mean W_{s-exp} of *S. costatum* aggregates >1000 - 2350 µm was higher by a factor 2 (0.6 ± 0.18 cm s⁻¹).

Incubation tank (W_{s-cal})

Calculated settling velocities of aggregate were generally higher than experimentally derived values ranging between 0.2 to 2.9 cm s⁻¹ (Fig. 21). W_{s-cal} was determined for particles of 208 to 5264 µm in diameter. No significant relationship was found between W_{s-cal} and particle diameter in *Exp I*. Mean values of W_{s-cal} for aggregates <1000 µm were measured to be 1.1 ± 0.7 cm s⁻¹. Mean W_{s-cal} of 1.5 ± 0.4 cm s⁻¹ were measured for aggregates >1000 - 2350 µm.

On the contrary, a significant relationship between calculated sinking velocities and particle diameter was found for *S. costatum* aggregates ($r = 0.55$, $P < 0.001$, $n = 38$). Mean velocities of both aggregate size classes were in the same range as reported for *Exp I*.

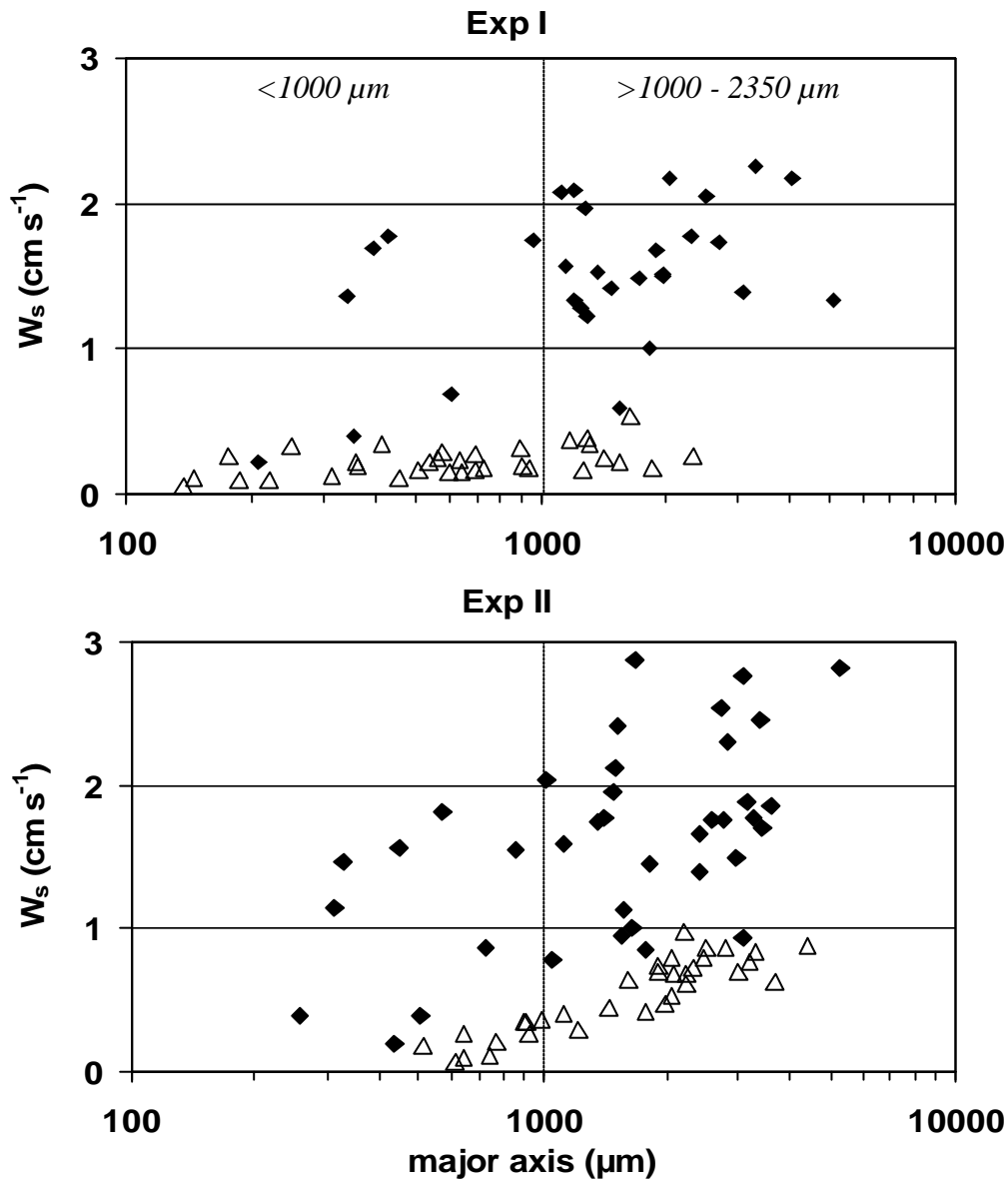


Fig. 21: Settling velocities derived from settling chamber measurements (W_{s-exp} , open triangles with $n = 33$) and calculated values from visible velocities during solid body rotation in the tank (W_{s-cal} , closed diamonds with $n = 30$ [Exp I] and $n = 38$ [Exp II]). In Exp I, no relationship was found between particle size and sinking velocity (W_{s-exp} and W_{s-cal}). *S. costatum* aggregates formed in Exp II showed significant positive relationships between particle size and W_{s-exp} ($r = 0.84$, $P < 0.001$, $n = 33$) as well as W_{s-cal} ($r = 0.55$, $P < 0.001$, $n = 38$).

Particle analysis

Table 3 summarises the results of various particle parameters in the replicate tanks of *Exp I*, without added diatom cells, and *Exp II*, with added diatom cells before (*SP*) and after roller table incubation (*W*; *A+W*). Numbers of *A* are calculated as the difference of *W* and *A+W*.

Values for total suspended particulate matter (*SPM*) in suspension (*SP*) were in the same range in both setups indicating that conditions in the tanks of both experiments are likely comparable. In both experiments, concentrations of all measured parameters showed higher values in *A+W* compared to *SP*. This may be an indicator of bacterial and algal growth during roller table incubation. Higher numbers of pennate diatom and bacteria cells support this notion (Tab. 4).

In *Exp I*, concentrations of *TPM*, *POC*, *PON* and photopigments (*Chl* and phaeopigments) showed higher values in the aggregate phase (*A*) compared to the water (*W*) after roller table incubation. Values of *Chl* in the aggregate phase exceeded those from the water by a factor 6. *POC* and *PON* were found to be higher by a factor 4 and 2.5, respectively. Parameters indicative of sticky particle (*TEP* and *CHE*) decreased in the aggregate phase (*A*).

In the suspension of *Exp II*, a slight increase of *POC*, *PON*, photopigments and *TEP* concentrations relative to *Exp I* was found demonstrating the influence of added cultured diatoms on particle composition. Lower concentrations of *CHE* were measured in the suspension compared to *Exp I*. At the end of the roller table incubation with *S. costatum*, carbohydrates (*CHE*) were preferably incorporated in the aggregates and concentrations in *A* exceeded those of the water overlying the aggregates (*W*). Considering the standard deviation of *TEP* concentrations, values of *W* and *A+W* were in the same range. Hence, *TEP* particles were found to be absent in aggregates (*A*) formed during *Exp II*.

Tab. 3: Characterisation of particles (mean \pm SE) in the samples taken during *Exp I* (upper table) and *Exp II* (lower table). *SP* – suspension before roller table incubation ($n = 1$, except *TEP* with $n = 3$), *W* – water overlying the settled aggregates in the tank after incubation ($n = 3$, except *TEP* with $n = 9$), and *A+W* – aggregates and water after incubation ($n = 3$, except *TEP* with $n = 9$). Values for aggregates (*A*) are calculated as the difference of *W* and *A+W*. *SPM* – total suspended particulate matter; *POC* – particulate organic carbon; *PON* – particulate organic nitrogen; *Chl* – chlorophyll a equivalents; *CHE* – colloidal carbohydrate equivalents; *TEP* – transparent exopolymer particles. “-“ values are negative.

Exp I	SP	W	A+W	A
SPM (mg Γ^1)	58.8	41.3 \pm 1.5	92.7 \pm 8.1	51.33 \pm 6.66
POC (mg Γ^1)	0.33	0.23 \pm 0.04	0.85 \pm 0.07	0.76 \pm 0.11
PON (mg Γ^1)	0.05	0.04 \pm 0	0.11 \pm 0.01	0.10 \pm 0.02
Chl (μ g Γ^1)	0.1	0.03 \pm 0.01	0.23 \pm 0.09	0.20 \pm 0.09
Phaeopigments (μ g Γ^1)	0.68	0.17 \pm 0.02	1.15 \pm 0.2	0.98 \pm 0.21
CHE (mg Γ^1)	1.55	1.35 \pm 0.1	1.76 \pm 0.43	0.41 \pm 0.39
TEP (mg Γ^1)	1.54 \pm 0.02	2.45 \pm 0.11	2.69 \pm 0.19	0.23 \pm 0.26

Exp II	SP	W	A+W	A
SPM (mg Γ^1)	55.2	41.3 \pm 1.5	92.7 \pm 4.2	51.33 \pm 4.51
POC (mg Γ^1)	0.49	0.21 \pm 0.01	1.29 \pm 0.15	1.08 \pm 0.15
PON (mg Γ^1)	0.07	0.05 \pm 0	0.19 \pm 0.04	0.14 \pm 0.03
Chl (μ g Γ^1)	0.14	0.06 \pm 0.01	0.46 \pm 0.11	0.40 \pm 0.11
Phaeopigments (μ g Γ^1)	1.07	0.27 \pm 0	1.81 \pm 0.19	1.54 \pm 0.19
CHE (mg Γ^1)	0.89	0.50 \pm 0.13	1.58 \pm 0.49	1.08 \pm 0.44
TEP (mg Γ^1)	1.94 \pm 0.25	3.13 \pm 0.6	2.81 \pm 0.17	-

Algae and bacteria cell abundance

Here, the terminology of the phases sampled before and after roller table incubations were taken over from table 3. Hence, cell numbers from the aggregate phase (A) were calculated from W and $A+W$.

Resuspended cells of pennate diatoms and bacteria were abundant in tanks of both experiments while cells of the diatom *S. costatum* were only found in water samples of *Exp II* (Tab. 4). Calculated values of A reveal that benthic and pelagic were incorporated into aggregates. About 40% of pennate cells from $A+W$ were found in aggregates (A) after *Exp I*, whereas at the end of *Exp II*, 70% were incorporated. 70% of *S. costatum* cells were embedded in A during *Exp II*.

Tab. 4: Algae and bacteria cell abundance from both experiments. Numbers of pennate diatoms and *S. costatum* cells are median values of two tanks. Bacterial abundance is given as mean \pm standard deviation with $n = 3$ tanks. Values for aggregates (A) are calculated from W and $A+W$. "n.d." denotes not determined and "--" values are negative.

	Exp I				Exp II			
	SP	W	A+W	A	SP	W	A+W	A
Pennate diatoms ($10^4 \Gamma^{-1}$)*	0.6	0.75	1.3	0.5	n.d.	0.4	1.4	1
<i>S. costatum</i> ($10^4 \Gamma^{-1}$)*	0	0	0	0	n.d.	0.65	2.34	1.7
Bacteria abundance ($10^8 \Gamma^{-1}$)*	1.7	7.8 ± 1.4	6.6 ± 3.0	-	4.9	5.4 ± 0.8	9.1 ± 1.9	3.7 ± 2.4

* cell numbers enumerated from subsamples of tank water

In *Exp I*, calculation of bacterial cell number for the aggregate phase revealed in a negative number whereas 40% of bacterial cells from *A+W* were incorporated in *A* at the end of *Exp II*. Diatom and bacterial biomass apparently increased during 18 h of both roller table incubations. At the end of *Exp I*, cell abundance of pennate diatoms and bacterial (*A+W*) increased by a factor 0.8 and 4.5 respectively, compared to the numbers in the suspension before roller table incubation (*SP*). After *Exp II*, cell abundance of bacteria doubled in *A+W* compared to *SP*.

Discussion

The present study aimed to describe transport behaviour of particulate matter in the *BBL* of the study area. The influence of microorganisms on (i) sediment erosion thresholds and (ii) aggregation as well as sinking behaviour of *in situ* sediment surface particles was assessed. In the context of micro-biostabilisation effects, living conditions of benthic phototrophs regarding the light environment in the study area will be conferred. Before discussing the presented results, methodological difficulties in terms of erosion threshold determination will be examined.

Determination of erosion thresholds – a critical examination

Two erosion thresholds were defined (see p. 15) in order to improve analysis of data deriving from microcosm experiments. Generally, erosion of non-cohesive sediments is often described as the simultaneous motion of single grains as outlined e.g. by Grant and Gust (1987) who defined erosion thresholds as the movement of 10 or more sand grains measured by observing the test section of the erosion device. Erosion of natural sandy, non-cohesive sediments is often influenced by biogenic structures, e.g. mussel shells, that alter hydrodynamic conditions and thus, influencing particle transport in the area of the biogenic structure (Eckman et al. 1981, Friedrichs 2003). In those areas that

comprise typically a few cm² only, rolling transport of single grains may be superimposed by integrated erosion behaviour of the sediment bed in the test section of the erosion device. In the microcosm the test section with 314 cm² is considerably larger. Once erosion of fine particles occurs at one point, the turbidity of the overlying water increases and further observation of the test section becomes impracticable.

The use of the observation method in terms of measuring erosion thresholds of cohesive sediments is also unpractical because surface particles are often invisible to the naked eye. As reported in the literature, sediment cohesion may occur at grain sizes <30 μm (Thomsen and Gust 2000), <20 μm (Mehta and Lee 1994), or <40 μm (Ackers and White 1973), and in sands with a content of the silt and clay fraction (<62.5 μm) of more than 15% by weight (Mitchener and Torfs 1996). However, while dealing with natural sediment surfaces a separation in cohesive and non-cohesive sediments does often not meet reality. Most natural cohesive beds have a fluffy, unstable surface layer showing non-cohesive transport behaviour. Therefore, Lavelle and Mofjeld (1987) argued that a threshold for cohesive beds does not exist because subunits within a flock of the fluffy layer will be transported at even very low shear stress velocities. To assess these primary transport processes of unconsolidated material on top of both mud and fine sand beds, a threshold of initial particle transport ($u^*_{cr-initial}$) was defined based on visual observation.

Erosion fluxes are widely used to obtain the threshold of erosion of surface particles that increase water turbidity. Mehta and Partheniades (1982) classified two types of particle erosion on the basis of differences in erosion, i.e. “Type I” and “Type II” erosion. The former is characterized by a pulse of material flux and an exponential decay of erosion flux with time after initial floc erosion. The latter describes constant erosion of a rather consolidated sediment surface. Amos et al. (1992) further described “Type I a” – resuspension of flocs at low shear stress velocities, and “Type I b” – resuspension of more consolidated aggregates. In this study, surface flocs and fine particles were predominantly eroded from natural sediment surfaces following “Type I” erosion showing the typical pattern described above (Fig. 6, p. 16).

Sediment erosion in the study area

Sediment cores of the mud station were characterised by an extensive, homogenous fluffy layer covering the consolidated bed and leading to a homogenous sediment topography at all sampling dates. Comparing the mineralogical composition of resuspended material from fine sand and mud cores revealed enhanced proportions of opal and mixed layer silicates such as illite at both sites (20% and 40% relative particle abundance, respectively). Mixed layer silicates have a pronounced affinity to organic substances and were found to be abundant in fluffy layer material (Leipe et al. 2000). This indicates sedimentation and deposition of organic particulate material along with minerals originated from coastal areas being laterally transported to the basin (Christiansen et al. 2002, Leipe et al. 2000). Moreover, fluff contributes to near bed lateral advection of organic pollutants (Witt et al. 2001) and was found to play an important role of particle flux in the deep sea (Thomsen and Van Weering 1998). It is a matter of debate whether or not the fluffy layer forms part of the bed (Amos et al. 1997). Nonetheless, there is a close link between fluffy layer properties and processes taking place in the sediment as already postulated (Pempkowiak et al. 2002, see below).

In the present study, particle sizes of fluff material remained undetermined. However, they are probably highly variable and often exceed mean diameters of underlying sediment grains (Thomsen and Gust 2000). Although, measurements of critical shear stress velocities for fluff across a range of environments show comparable results (Tab. 5).

Tab. 5: Critical shear stress velocities of fluff. Numbers presented for the this study refer to mean values of $u^*_{cr-initial}$ and $u^*_{cr-erosion}$ of mud cores ($n = 6$) covered by fluff.

u^*_{crit} (cm s ⁻¹)	Method	Author
0.4 - 0.6	Microcosm	this study
0.8 - 0.9*	Microcosm	Thomsen and Gust (2000)
0.4 ^b	indirect	Laima et al. (1999)
0.4 - 0.5 ^a	Laberex chamber	Lund-Hansen et al. (1999)
0.7 - 1.0 ^a	Sea Carousel	Maa et al. (1998)
0.4 ^b	indirect	Sanford et al. (1991)
0.4 - 0.9	Seaflume	Gust and Morris (1989)

^a Values were transformed from the original data set.

^b Values calculated from current velocity measurements.

* mean values

At the mud site, the flocculent layer was responsible for particle transport. Figure 22 illustrates a high density of surface flocs in the overlying water of a mud core during an erosion experiment. Comparing erosion thresholds based on Shields and Hjulström parameters (Eqs. [3], [5], [8] and [9]) and experimentally derived thresholds for mud cores, grain size as reference base is questionable (Fig. 13, p. 36). On the other hand, eroded particles at the fine sand station were likely comparable to mean-sized particles because fluffy material occurred in relatively low amounts ($u^* = 1.2$ cm s⁻¹). Nevertheless, fine sand cores taken in September 2000 and April 2001 were eroded under critical shear stress velocities lower than the mean value ($u^*_{cr-erosion} < 1.0$ cm s⁻¹). This indicates erosion of unconsolidated, fluffy material at the fine sand station too. Since $u^*_{cr-erosion}$ for fluff in the present study as well as in the literature (Tab. 4) were found to be ≤ 1.0 cm s⁻¹, this value may be regarded as a uniform threshold to identify fluff material via erosion behaviour.

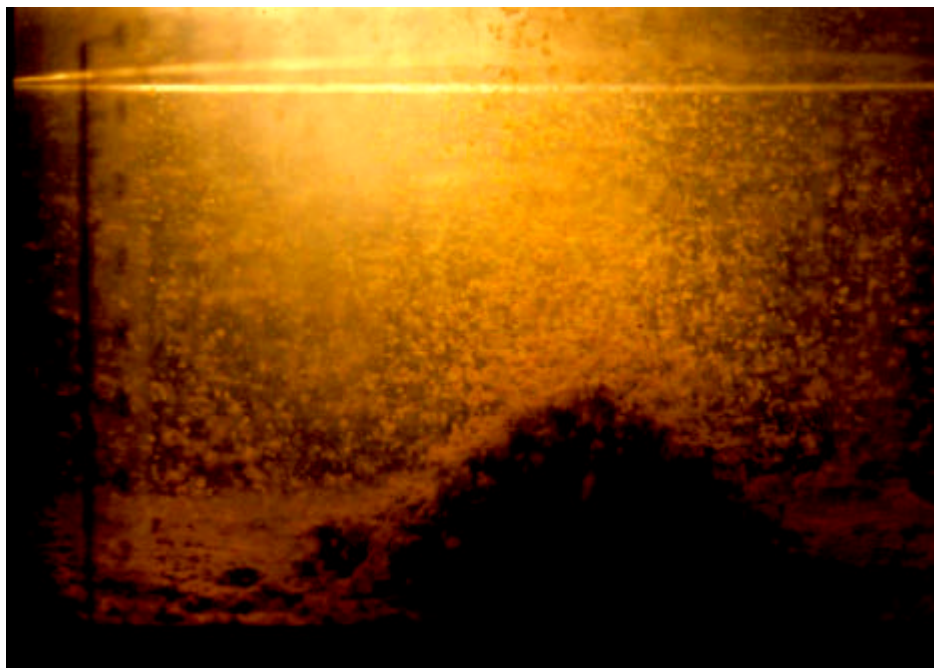


Fig. 22: Floc erosion during a microcosm experiment with a core taken at the mud station. Flocs being not yet resuspended were transported and deposited in the centre of the core forming a cone of sediment. The stirring disc of the device appears in the upper part of the picture.

Fluff dynamics in the study area has to be seen as an important process coinciding highest values of erosion flux at both sites. This is expressed with the significant negative correlation between values of $u^*_{cr-erosion}$ and erosion flux at both sites. So, a higher mass of particulate mater is mobilized at low shear stress velocities.

Fluff erosion may occur on a wide area in Mecklenburg Bight because the investigated sediment types, fine sand and mud, cover about 80% of the study area (Bohling 2003). Therefore, for the purpose of modelling sediment transport it is necessary to use sediment types rather than mean grain sizes.

Variations of erosion thresholds and micro-biostabilisation effects

Variations of erosion thresholds measured at both sites during the investigation has to be considered in the understanding of biogenic influences on sediment stabilisation.

Seasonal variations of critical shear stress velocities were also found by Krögel (1997) who inferred that processes of sediment dynamics depend on the viscosity of the fluid, and therefore on temperature. Further insights of physical and sedimentological influences on sediment transport in the investigation area are given by Bohling (2003). Moreover, particle transport of coastal beds is dependent on both stabilisation and destabilisation effects of sediment-inhabiting organisms (e.g. Krumbein et al. 1994, Paterson and Black 1999).

In order to assess the influence of benthic diatoms on the observed erosion behaviour, concentrations of biochemical sediment parameters indicative of microbial biomass and biogenic exudates were correlated with erosion thresholds (Tab. 2, p. 42). Beside the water content, *Col S* remained the only parameter showing significant correlations with $u^*_{cr-initial}$ and $u^*_{cr-erosion}$. This relationship agrees with findings of numerous authors calculating significant positive relationships between erosion thresholds and colloidal carbohydrates and thus, predicting micro-biostabilisation effects on intertidal sediment surfaces (Grant and Gust 1987, Underwood and Paterson 1993, Sutherland et al. 1998, Christie et al. 2000, Yallop et al. 2000). Generally, stronger relationships between sediment parameters and erosion thresholds were found at the mud station compared to fine sand station. This was likely caused by differences in sediment surface topography of the sampled cores as described above. The homogenous topography resulted in low variations of sediment parameters (Fig. 15 and 16, p. 39 and 40) and erosion thresholds. Surfaces of fine sand cores were covered by biotic and abiotic structures such as ripples with varying extension over the sampling period. This topography may evoke a patchy distribution of sediment properties and microbenthic biomass on the sampling area of the box-corer. Sundbaeck (1984) and Glud et al (2002) found variations of diatom biomass on a spatial scale of metres. Grant et al (1986 b) described patchy distribution of *Chl* on a centimetre scale. In the later study, selective rolling transport and entrainment of exposed sand particles attached with algae on ripple crests induced a patchy distribution of photopigments. This may be true for the fine sand station in the investigation area although, in September 2000, *Chl* was found to be normally distributed about the mean ($n = 13$, $p < 0.05$). However, as *Chl* and abundances of diatom cells show high discrepancies at both sites in January 2002 patchy distribution of sediment parameters can not be excluded.

Values of *Chl* did not significantly correlate with either *Col S* and *Col EDTA*. A lack of correlation reveal that the source of carbohydrates at both sites remained unidentified. Other studies illustrate that the relationship between these parameters is not simple. While a significant correlation between *Col EDTA* and *Chl* was reported by Van Duyl et al. (2000), only the loosely bound fraction of carbohydrates extracted with water correlated with diatom biomass in the work of De Brouwer et al. (2000). Supporting the present results, no relationship between exudates and chlorophyll *a* was found by Madsen et al. (1993). Several reasons may cause these discrepancies.

Microorganisms produce exudates on the sediment surface that have a short half-life, being rapidly hydrolysed in the presence of water (Edgar and Pickett-Heaps 1984, Paterson 1990). On intertidal mudflats this effect was observed during low tide on ripple troughs where sediment water content was high compared to ripple crests. In the crests, air exposure prevented hydrolysis of carbohydrates (Blanchard et al. 2000). Madsen et al. (1993) stressed that hydrolysis of sediment carbohydrates will be more pronounced in subtidal areas because water is always present.

A lack of the above mentioned relationship may also be caused by migration behaviour of benthic diatoms. The microphytobenthos shows vertical migrations in both subtidal and intertidal sediments on a centimetre scale (Saburova and Polikarpov 2003). Thus downward migration may reduce diatom biomass in the upper 5 mm of a sediment core increasing the discrepancy between chlorophyll *a* and colloidal carbohydrates remaining in the surface horizon.

Furthermore, the content of algal biomass and colloidal carbohydrates on sediment surfaces may be affected by benthic grazer and bioturbators. The mud snail *Hydrobia ulvae* is known to feed on benthic diatoms decreasing erosion thresholds of sandy sediments (Andersen et al. 2002). On the other hand, benthic meio- and macroorganisms generate exudates (Meadows and Tait 1989, Blanchard et al. 1997, Mouritsen et al 1998) increasing the content of carbohydrates. Finally, bacteria also contribute to the *EPS* pool (Decho and Moriarty 1990).

In the present study, it was not possible to specify the sources of *Col S* and *Col EDTA* because exudates widely consist of carbohydrates being measured as glucose equivalents by the quantification method used here. In order to improve interpretations

of the results of *EPS* equivalent measurements several authors suggested microtechniques for sampling sediment surfaces on a micrometer scale followed by Low-Temperature Scanning Electron Microscopy (e.g. Paterson 1995, Wiltshire 2000).

The major conclusion deriving from results of table 2 is that micro-biostabilisation remains unproven at both investigated sites. In this context the question arises whether environmental conditions in the investigation area allow phototrophic growth and thus, production of *EPS* by benthic diatoms.

Sediment samples were examined under the microscope revealing higher numbers of diatom cells with visually intact chloroplasts at the fine sand station compared to the mud station in July and October 2001, respectively. Cell numbers found here correspond to diatom abundances determined in Laholm Bay, south-eastern Kattegat, monitored over a period of one year in water depths of 0 – 30 m (Sundbaeck 1986, Sundbaeck and Joensson 1988). Sundbaeck (1986) found highest rates of benthic primary production in 14 – 16 m water depths with light intensities of $20 \mu\text{E m}^{-2} \text{s}^{-1}$. Generally, phototrophic growth and thus diatom abundances are limited by light conditions which are reduced in lower subtidal areas compared to tidal mudflats. In these light saturated environments both photosynthesis and production of exudates were found to be strictly connected (Smith and Underwood 1998, De Winder et al. 1999, Staats et al. 2000). Light conditions in the environment of the investigation area are different and will be discussed below.

Average values of *PAR* still permitting phototrophic growth are given as $5 - 10 \mu\text{E m}^{-2} \text{s}^{-1}$ (Cahoon 1999). In an arctic fjord, Glud et al. (2002) demonstrated that benthic diatoms quickly optimize their photosynthetic apparatus to changing light conditions down to $4.5 \mu\text{E m}^{-2} \text{s}^{-1}$ confirming the values of Cahoon (1999). However, studies dealing with micro-biostabilisation effects of sediment surfaces reported increased *EPS* content and thus, erosion thresholds under higher *PAR* values. In a laboratory experiment benthic diatoms sampled from a shallow subtidal area at 0.6 m water depth significantly increased erosion thresholds after being incubated at $200 \mu\text{E m}^{-2} \text{s}^{-1}$ (Madsen et al. 1993).

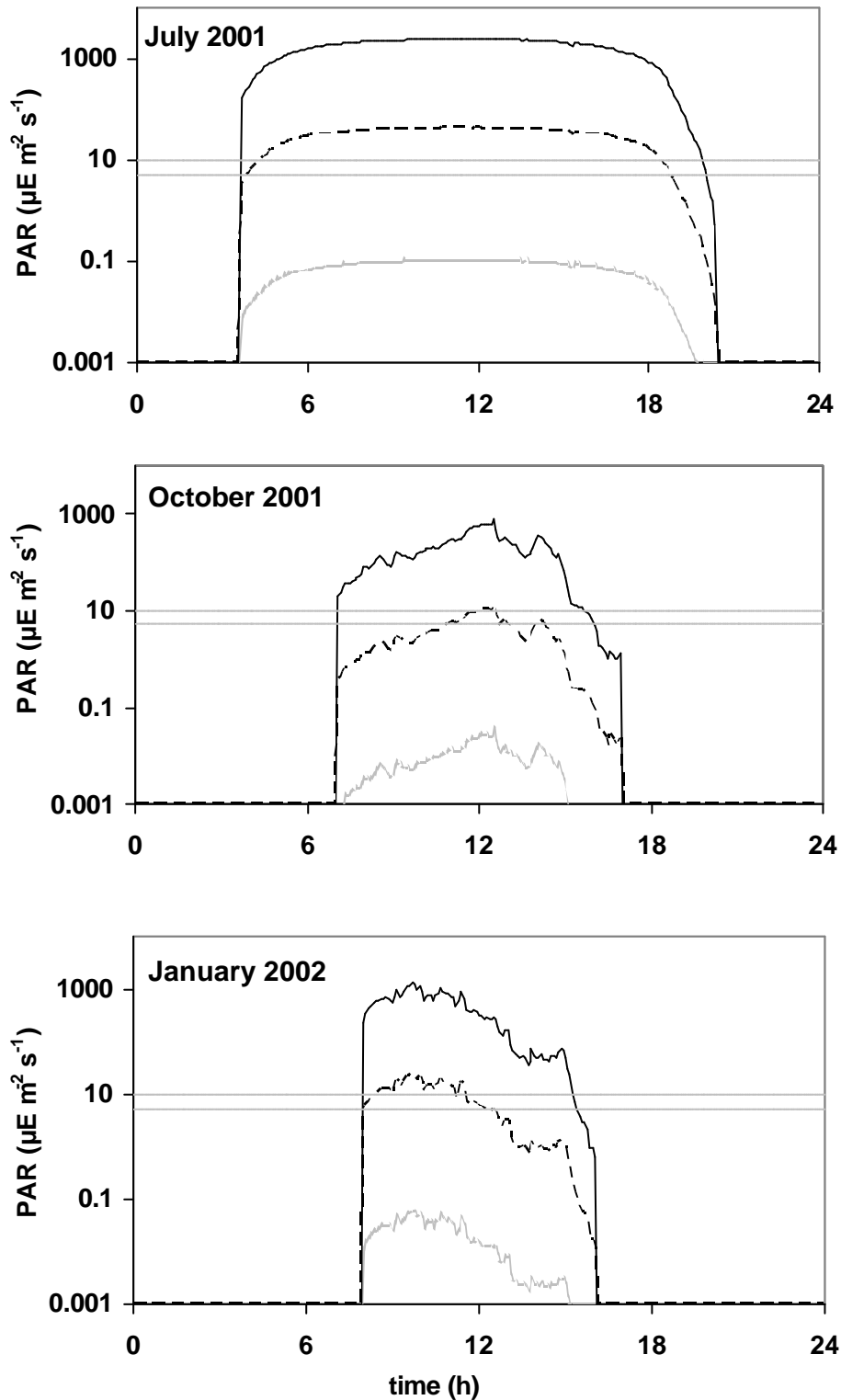


Fig. 23: Subsurface light intensities (solid lines) calculated from surface *PAR* measured on board and calculated *PAR* at the bottom (20 m water depth) using an attenuation coefficient of 0.2 (dashed lines) and 0.5 (dotted lines). Horizontal boxes indicate lower limit of *PAR* permitting phototrophic growth (Cahoon 1999; see section of Material and methods for calculations).

Light intensities predominating at the seafloor of the investigated sites are of the order and even less than average values given by Cahoon (1999). In this context it is important to mention that calm and sunny weather conditions occurred at the sampling day in July 2001. Thus, optimal illumination occurred supported by low variations of *PAR* intensities (Fig. 23). At the following two occasions light intensity and duration decreased at the surface and the bottom of the water column (Fig. 5). Therefore, environmental conditions supporting photosynthesis and *EPS* production became suboptimal in October 2001 and January 2002 compared to July 2001. Contrarily, highest diatom cell abundances were found at both sites in January 2002 increasing by a factor 3 at the fine sand station and a factor 6 at the mud station (Fig. 17, p. 41). In agreement with this, $u^*_{cr-erosion}$ and *Col S* show highest values at the fine sand station in January 2002 (Fig. 2). These findings may be an indicator of micro-biostabilisation effects at this sampling site and occasion. However, values of $u^*_{cr-erosion}$ and *Col S* were found to be higher in October compared to July 2001 being in disagreement with diatom abundances.

What mechanism may have caused the observed patterns of diatom abundances? Considering the results of *PAR* measurements, increasing diatom cell numbers can hardly be explained with an on-site growth at water depths of approximately 20 m in the investigation area. It is more likely to assume that hydrodynamic forces inducing resuspension of benthic diatoms from shallow subtidal areas (De Jonge 1985, De Jonge and Van den Bergen 1987, Sundbaeck and Joensson 1988, Wiltshire et al 1998) and followed by lateral transport of benthic algae within the fluffy layer, finally depositing algae in the basin of Mecklenburg Bight. Microscopical examination of experimentally resuspended surface material from the mud site revealed pennate diatom cells incorporated into fluffy layer material supporting this hypothesis (Fig. 24). This mechanism would explain higher cell abundances at the mud station compared to the fine sand site in January 2002.

Although, diatoms are known to be capable of heterotrophic growth (Admiraal and Peletier 1979) and *EPS* production in the dark (Underwood and Smith 1998) the influence of microphytobenthos on sediment stability at water depths ≈ 20 m may virtually be excluded. At water depths equal to the investigated sites, results of *PAR* measurements point out that net photosynthesis and production of exudates may be

restricted to calm weather with optimal light conditions. At shallower areas of Mecklenburg Bight, e.g. <5 m, values of *PAR* may reach those reported by Madsen et al. (1993) during most of the day. Although, little is known about microphytobenthos abundance in these shallow areas phototrophic growth and micro-biostabilisation of sediment surfaces are likely to be limited to these shallow subtidal habitats. They encompass approximately 10% of the total area of Mecklenburg Bight. Thus, 90% of the area remains little affected by micro-biostabilisation of phototrophic diatoms.

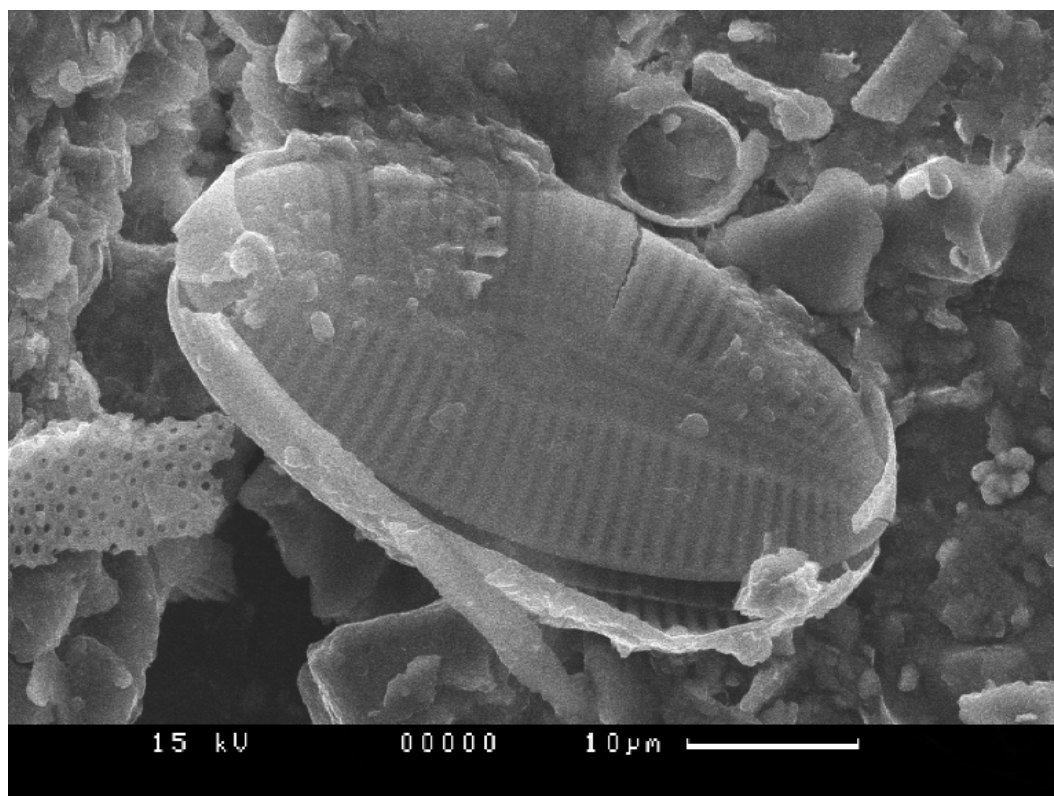


Fig. 24: Scanning electron microscope photograph of a pennate diatom cell within fluffy layer material. The cell is surrounded by thin layer possibly of organic origin.

Aggregation behaviour of resuspended particles

Beside the investigation of resuspension behaviour of natural sediment surfaces, aggregation and settling behaviour were experimentally examined in plexiglass cylinders rolling horizontally (Shanks and Edmondson 1989). A camera system (i) documented and measured aggregate formation during incubation as described by Jähmlich and Graf (1998) and (ii) determined settling velocities during solid body rotation (Engel and Schartau 1999). Settling velocities were independently measured in a settling cylinder.

Results from roller table experiments with naturally resuspended particles (*Exp I*) and added planctonic algae (*Exp II*) show that particle sizes significantly increased during the first six hours of incubation. After this initial growth phase, particles from both experiments showed a diverging aggregation behaviour (Fig. 19 and 20, p. 45 and 46). These findings correspond to the results of Jähmlich and Graf (1998) who experimentally determined growth rates of aggregates forming in water samples taken from the *BBL* of Mecklenburg Bight. They found initial growth for 10 hours and subsequent stagnation of mean aggregate diameters. The authors argued that differences in particle composition led to different growth rates.

Here, particle composition has been changed in *Exp II* deliberately by addition of *S. costatum* cells. Accordingly, concentrations of particulate carbon, nitrogen and photopigments were higher in *Exp II* in the suspension and in aggregates compared to *Exp I*. Air bubbles, as a cause of stagnating aggregate growth, were not visible in the tanks throughout the incubation and thus, disaggregation effects (Jackson 1990) as discussed by Jähmlich and Graf (1998) may be neglected.

To conclude, *S. costatum* cells influenced rate and efficiency of coagulation of particles in the tanks resulting in a continuous growth during the whole incubation time. This also leads to aggregate diameters reached highest values in *Exp II*.

The role of phytoplankton cells in the formation of macroscopic aggregates is well reported in the literature. Especially cells of *S. costatum* that produce exopolymeric substances are described to be highly sticky (Kioerboe et al. 1990, Kioerboe and Hansen 1993, Engel 2000). This species is known to contribute to the *TEP* pool in the water

column during phytoplankton spring blooms and was found to be abundant in macroscopic aggregates (e.g. Alldredge et al 1993, Passow and Alldredge 1995 a). Microscopic examinations of aggregates showed a high abundance of *S. costatum* cells, bacteria and pennate benthic diatoms in *Exp II*. A lower number of pennate diatom cells and no bacteria were found in the aggregates of *Exp I* (Tab. 4, p. 51). These results show that in the presence of *S. costatum* entrainment of bacteria and pennate diatoms into aggregates was enhanced.

Concentrations of parameters indicative of sticky particles (*TEP*, *CHE*) were expected to elucidate this process. *TEP* were present in the samples with slightly higher values in *Exp II* compared to *Exp I* (Tab. 3, p. 50). At the end of both roller table incubations concentrations of “stickiness”-parameters did not reflect bacteria and diatom cell abundances in the aggregate phase. This inconsistency with the entrainment of bacteria and benthic diatoms may result from methodological artefacts.

The quantification of *TEP* particles is highly depended on anionic groups specific to chemical compounds (Engel and Passow 2001). This may cause discrepancies of field and laboratory results (Passow and Alldredge 1995 a). Engel and Passow (2001) presented *TEP* concentrations in the euphotic zone of the Baltic Proper that were up to 30-fold higher compared to the results from our experiments that were in a range of a fresh diatom culture (Engel 2000). Moreover, acidic polysaccharides can be enclosed by inorganic particles in the aggregates reducing complexation with the dye used. Thus, concentrations of *TEP* particles will be underestimated especially in the aggregate phase. This underestimation is likely to be true also for the determination of *CHE*. Generally, the method used for the quantification of *CHE* is not suitable for distinguishing between intra- and extracellular polysaccharides, but it is well established as a method for the determination of *EPS* equivalents in marine (Underwood et al. 1995) and limnic sediments (Liu et al. 1973).

For further aggregate studies ultrasonic pre-treatment and hence, disaggregation of investigated flocs may release a higher amount of stainable particles (*TEP*, *CHE*) in the aggregate phase.

So far, the role in the formation of aggregates of resuspended pennate diatoms and bacteria from the seafloor has not been sufficiently investigated. As discussed above, benthic diatoms produce *EPS* that will necessarily be entrained into the overlying water attached to resuspended particles as shown for photopigments after sediment erosion by Wiltshire et al (1998). Bacteria are also known to produce exopolymeric substances (Decho 2000). The synthesis of *EPS* is stimulated in bacteria attaching to surfaces (Vandevivere and Kirchman 1993), such as aggregates, and may increase particle stickiness in the *BBL*.

In both experiments pennate diatoms as well as bacteria were attached to sediment particles after resuspension increasing particle stickiness and acting as coagulation kernels. In the absence of *S. costatum* cells the majority of attached benthic sticky cells might be enclosed by inorganic, less sticky particles after 6 hours incubation time resulting in a stagnation of aggregate growth as determined in *Exp I*. On the other hand, sticky particles were more abundant in *Exp II* because of added diatom cells. During roller table incubation, cells of *S. costatum* collided with aggregates of benthic diatoms, bacteria and inorganic matter sticking to their outer edge. Hence, coagulation efficiency was high and aggregate size significantly increased during the whole incubation time of *Exp II*.

Settling velocities and particle residence time in the *BBL*

Settling velocities were measured with two methods providing a view of aggregate settling behaviour according to compositional changes. Results presented in figure 21, page 48, illustrate that settling velocities determined during solid body rotation in the tank (W_{s-cal}) exceed those from measurements in the settling chamber (W_{s-exp}).

The discrepancy of W_{s-cal} and W_{s-exp} can be caused by different factors. Generally, numerous methods were used to determine settling velocities either *in situ* or in the laboratory (Alldredge and Silver 1988, Puls and Kuehl 1996, Diercks and Asper 1997). Engel and Schartau (1999) developed a method to measure settling velocities *in vitro* without affecting aggregate shape and size. This is in contrast to Jähmlich and Graf (1998), where the use of a syringe transferring aggregates to a settling chamber implies

potential compaction of aggregates. This could lead to decreasing porosity, increasing density and thus increasing settling velocity of aggregates (Alldredge and Gotschalk 1988). On the other hand, disaggregation effects are likely to occur using a syringe. The appearance of smaller particle sizes in W_{s-exp} compared to W_{s-cal} of *Exp I* may be a sign of such an artefact.

Aggregates recorded with the video camera system in the tank of *Exp I* tended to be more porous than *S. costatum* aggregates (see below). Because the sampling procedure using a syringe may lead to aggregates more uniform in porosity and density, values of W_{s-exp} show much reduced variation compared to W_{s-cal} .

Length measurements for aggregate position in the x-y plane of the tank effecting values of W_{s-cal} may also be seen as a limit to the accuracy W_{s-cal} determination. An overestimation of 2 mm in the radial distance of aggregate position to the centre of the tank would increase W_{s-cal} by 0.1 cm s^{-1} compared to the presented results. Therefore, W_{s-cal} determination can be seen as sufficiently accurate for further comparisons because variances in W_{s-cal} of similar sized aggregates were higher than 0.1 cm s^{-1} .

Aggregate composition influenced settling velocities of both W_{s-cal} and W_{s-exp} with values exceeding those presented in the literature. Numerous empirical functions were reported relating aggregate size to velocity (Gibbs 1985, Alldredge and Silver 1988). This relationship was specially found for marine snow aggregates containing high numbers of pelagic diatoms cells (Alldredge and Gotschalk 1988). Recently, a rather uniform value of *in situ* floc sinking speed of 0.1 cm s^{-1} was proposed by Hill and Mc Cave (2001) who compared *in situ* measurements dealing with a wide variety of environments and aggregate geometries. In agreement with this latter hypothesis, W_{s-exp} and W_{s-cal} of aggregates formed in *Exp I* did not increase significantly with particle size. On the contrary, addition of *S. costatum* to aggregates resulted in a positive significant relationship between settling velocity and aggregate size (*Exp II*).

Aggregates formed containing pennate diatoms (*Exp I*) and both pennate diatoms and *S. costatum* (*Exp II*). Apart from higher diatom cell abundances, concentrations of photopigments as well as *POC* and *PON* were increased in the aggregate phase of *Exp II* compared to *Exp I*. Aggregates with many diatom cells may have a higher average

density, resulting in higher settling velocities compared to inorganic flocs as proposed from *in situ* (Thomsen and McCave 2000) and laboratory observations (Beaulieu 2003). Engel and Schartau (1999) support these findings and present values of excess density of diatom aggregates up to 2 orders of magnitude higher compared to natural flocs. Furthermore, excess density of diatom aggregates were found to increase with increasing lithogenic matter (Hamm 2002). Assuming a higher aggregate density in *Exp II*, the significant relationship between particle size and settling velocity can be explained (Fig. 3).

Pathways of resuspended particles (resuspension loops)

In order to relate the present laboratory results to particle transport from the sediment surface into the overlying water and within the *BBL*, hydrodynamic conditions in the *BBL* have to be noted. The critical size of flocs in a specific turbulence regime like the *BBL* is supposed to be regulated by the diameter of the smallest possible eddy, expressed by the *Kolmogorov length scale* (Eisma 1993) as $L = (\nu^3/e)^{1/4}$, where ν is the kinematic viscosity of the fluid and e stands for the turbulent energy dissipation. The latter parameter can be estimated as follows: $e = u^{*3}/k z$, where z is the height above seafloor and k the Karmans' constant. In this calculation mean critical shear stress velocity for this sediment type of $u^{*_{cr-erosion}} = 1.2 \text{ cm s}^{-1}$ (see above) was used. Values of L varied between 1000 and 2000 μm from 0.1 to 5 m above the sediment. Thus, turbulent conditions in the *BBL* at the given critical shear stress velocity would allow formation of aggregates with particle diameters as large as measured in roller table experiments.

Assuming that mean aggregate sinking velocities of 0.2 cm s^{-1} and 0.6 cm s^{-1} (W_{s-exp}) prevail in the field, calculated residence times of aggregates, formed at 5 m above the sediment (Turnewitsch and Graf 2003), would range between 15 to 40 min. Lowest residence times are calculated for *S. costatum* aggregates of 1000 – 2400 μm in diameter. Using mean values of W_{s-cal} , calculated residence times would decrease down to 5 – 8 min. Aggregate formation in the euphotic zone, 20 m above the seafloor, would lead to roughly 4-fold higher residence times.

On the other hand, measured growth rates for *S. costatum* aggregates generally do not allow *in situ* aggregate growth reaching 1000 μm particle diameter within the calculated residence time. *In situ* aggregate size measurements in the *BBL* of coastal areas reveal mean aggregate diameter less than 1000 μm , (Jähmlich and Graf 1998, Christiansen et al 2002, Jähmlich et al 2002). However, this does not exclude the existence of larger aggregates. Those exceeding 1000 μm in diameter with enhanced settling velocities were not included in the measurements of (Jähmlich et al 1999, Jähmlich et al 2002) who observed *in situ* particles from a water volume of only $1.9 \pm 0.1 \text{ cm}^3$ with a video camera system.

In the *BBL* of a deep sea area, larger organic rich aggregates reaching 2000 μm in diameter were observed (Thomsen and Gust 2000, Thomsen and McCave 2000). Here, particles reaching the seafloor had higher scavenging residence times ($^{234}\text{Th}/^{238}\text{U}$) compared to those from coastal waters (Turnewitsch and Springer 2001). However, calculated residence times for aggregates in this study may be underestimated because they derive from aggregate settling velocities measured under non-turbulent conditions. Kersten et al. (1998) measured residence times of approximately one week for particles in bottom waters of Mecklenburg Bight based on $^{234}\text{Th}/^{238}\text{U}$ disequilibria method. The corresponding settling velocities for these particles would be 2 orders of magnitude lower than mean values presented in this study. It has to be noted that the calculations of Kersten et al. (1998) are based on samples of suspended particulate matter including a wide range of particle sizes. Fine particles clearly decrease mean residence times and thus reduce the comparability of the results.

Flow induced particle flux is of great importance in order to model sediment dynamics. Erosion rate measurements can be used to estimate these fluxes. A maximum erosion rate of $5 \times 10^{-5} \text{ kg m}^{-2} \text{ s}^{-1}$ per 10 min incubation time at $u^* = 2 \text{ cm s}^{-1}$ was measured at the fine sand station in January 2002 resulting in particle entrainment of 30 g m^{-2} during this single erosion event (see Material and methods for calculation, p. 17). Assuming a resuspension height of 5 m above the seafloor, resuspended particles will be suspended in a water volume of 5000 l over an area of 1 m^2 . This would lead to an increase of suspended particulate matter concentration of 6 mg l^{-1} .

However, calculated shear stress velocities induced by measured and modelled flow velocities (u^*_{flow}) rarely exceed shear stress velocities of 2 cm s^{-1} (Fig. 14, p. 37). As a result, mass particle transport is largely controlled by storm events as reported by other authors for different aquatic environments (Maa et al. 1998, Poulos 2001). Erosion rates measured at lower critical shear stress velocities (mean $u^*_{cr-erosion}$ of fine sand = 1.2 cm s^{-1}) revealed an entrainment of 0.5 g m^{-2} resulting to an input of *SPM* concentration within the above mentioned water volume of $\leq 0.1 \text{ mg l}^{-1}$. This value is up to two orders of magnitude lower than *in situ* concentrations of *SPM* measured in the *BBL* of the investigation area (Jählich et al 1999). In this context, the influence of benthic macroorganisms contributing to particle flux via direct resuspension and deposition (Graf and Rosenberg 1997) is of great importance. However, the input of *SPM* concentrations by bioresuspension has not been quantified yet in the investigation area but is the major objective of an ongoing study (Peine pers. comm.).

The presented results of laboratory experiments provide some information about concurrent mechanisms of particle transport and thus, dynamics of organic material from coastal areas to the basin (Fig. 25). While stabilisation effects of benthic diatoms on sediment surfaces have to be neglected at the investigated sites, particle aggregation and transport in the *BBL* is highly influenced by sticky, pelagic algae. Aggregates including pelagic diatoms were found to have lower residence times compared to those without diatom cells. As a consequence, this implies a higher number of deposition events of organic rich aggregates and therefore interactions with the benthic element cycling may increase in shallow waters. The latter process was demonstrated by Pempkowiak et al. (2002) who found distinct particle exchange between fluffy layer material and the underlying sediment. Thus, fluff deposited under calm flow conditions is subject to mixing processes at the sediment surface such as bioturbation. Aggregates containing few biological components may be predominant in the formation of cohesive sediments because of their transport behaviour involving longer residence times. In the winter, when feeding activities of benthic macroorganisms are low compared to the summer, aggregates containing minerals as well as pelagic and benthic algae may longer remain in resuspension. Both aggregate types will then be transported and deposited in the basin. Results of benthic diatom abundances in sediments of the mud station may indicate this.

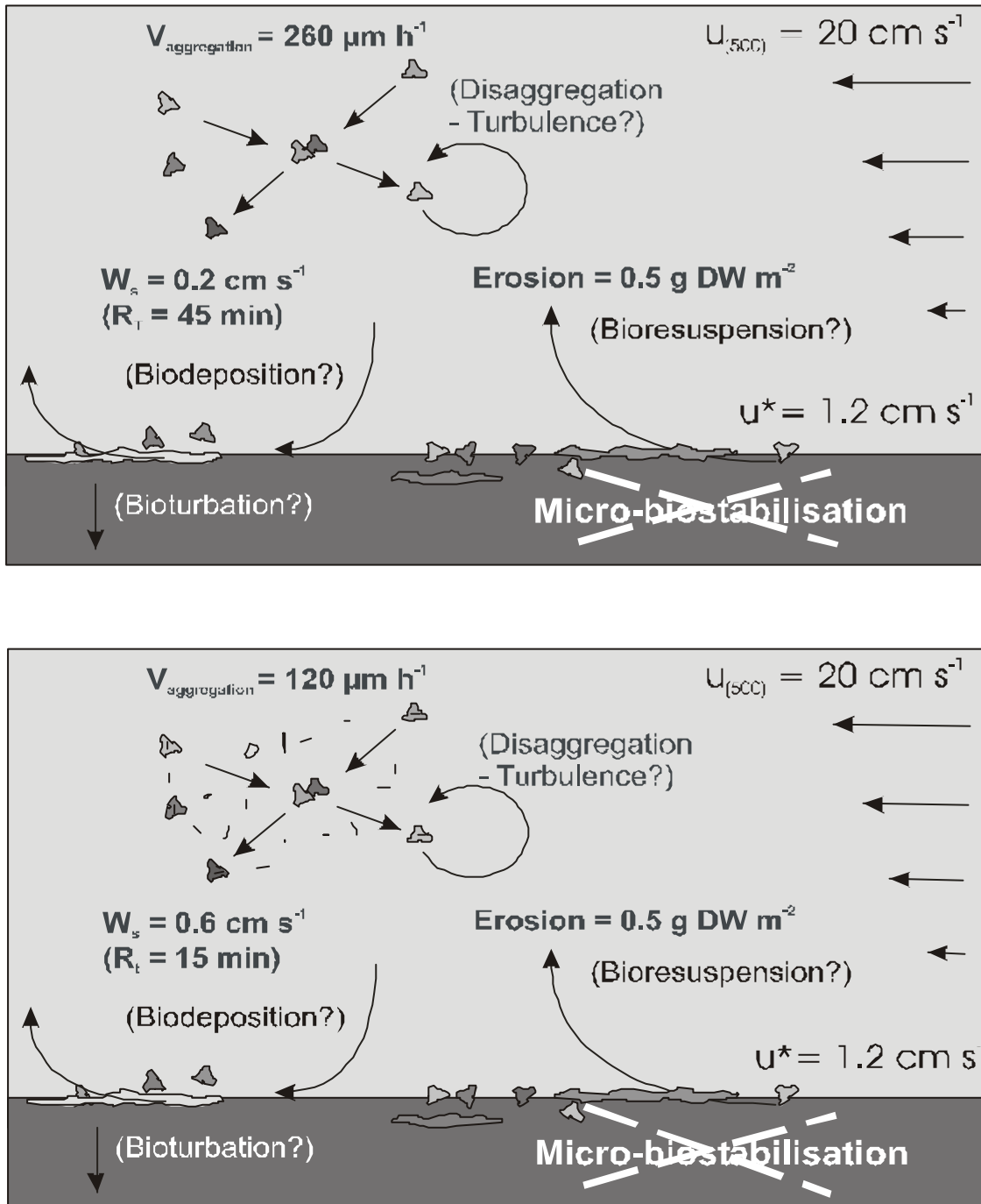


Fig. 25: Experimentally determined values influencing particle transport behaviour at the fine sand station. Micro-biostabilisation has to be neglected. Erosion conditions in both sketches are identical (right side). Aggregates including diatom cells (cells are indicated as lines) have a higher mean sinking velocity and thus, lower residence times in the water column (lower scenario).

The present knowledge is inadequate to predict details of resuspension loops of aggregated organic and inorganic material on its way from coastal areas to deposition sites in the basin. In the *BBL* particles are carried upwards by turbulence (Hill and McCave 2001), ensuring an increase of particle residence time. Furthermore, aggregation and disaggregation effects become hardly predictable. In the present context, the turbulence regime acting on aggregates in the BBL could not be assessed. Nevertheless, a considerable vertical turbulent transport has to be considered because of the high discrepancy of settling velocities presented here and *in situ* residence times. Computation of apparent settling velocities, resulting from a combination of turbulent transport and settling velocities, would provide a better mechanistic understanding of aggregate transport in coastal waters and should be subject of further investigations in this field.

Summary

This study aimed to describe erosion flux from the sediment surface into the overlying water and aggregation behaviour as well as sinking velocities of natural sediment surface particles. The influences of benthic and pelagic microorganisms producing exopolymeric substances on the sediment surface (*EPS*) and in the water column (*TEP*) were assessed. Samples were taken from a coastal fine sand station (19 m water depth) and a mud station (25 m) located in the basin of Mecklenburg Bight, south-western Baltic Sea. Both fine sand and mud represent the two dominant sediment types covering about 80% of the study area.

Erosion experiments were carried out using the erosion chamber microcosm at five different times of the year. Two thresholds of particle transport were defined ($u^*_{cr-initial}$ and $u^*_{cr-erosion}$) illustrating significant positive correlations at both sites and at all sampling occasions.

At the mud station, an unconsolidated surface layer (fluff) was present and responsible for particle transport at all sampling dates. On the other hand, fluffy material occurred in relatively low amounts at the fine sand site too. Here, the mean threshold of $u^*_{cr-erosion}$ (1.2 cm s^{-1}) was comparable to literature data for critical shear stress velocities based on grain sizes ($u^*_{cr-Shields}$ and $u^*_{cr-Hjulström}$). However, at two occasions, loosely bound material on top of the fine sand cores was abundant showing critical shear stress velocities lower than the mean value. As values for fluff erosion in the present study as well as in the literature were $\leq 1.0 \text{ cm s}^{-1}$, this value may be regarded as a uniform threshold to identify fluff material via erosion behaviour. Considering mass transport from the sediment into the overlying water, fluff erosion was found to be the dominant process in the study area.

During the sampling period between September 2000 and January 2002, the values of $u^*_{cr-erosion}$ showed higher variations at the shallower fine sand station (factor 2.4)

compared to the mud station (factor 2). Considering biostabilisation of benthic diatoms on sediment surfaces, positive correlations were found between erosion thresholds and concentrations of water soluble colloidal carbohydrates (*Col S*), indicating *EPS*. As benthic diatom biomass showed no positive correlations with *Col S*, the source of exudates remained undetermined. Both measured and calculated light conditions at the investigated sites illustrate that net photosynthesis and production of exudates may be restricted to calm weather with optimal light conditions. Micro-biostabilisation effects of sediment surfaces are limited to shallow areas with water depths <5 m, where irradiance is adequate to allow phototrophic growth (>5 - 10 $\mu\text{E m}^{-2} \text{s}^{-1}$). Thus, 10% of the total area of Mecklenburg Bight may be influenced by micro-biostabilisation effects whereas 90% of the area remains little affected.

In the benthic boundary layer (*BBL*), cells of benthic diatoms attached to sediment grains interact with organic material and minerals forming macroscopic aggregates. Experimentally formed aggregates with natural sediment surface particles and added cells of pelagic diatoms (*Skeletonema costatum*) showed increased rate and efficiency of particle coagulation compared to original material with natural microorganism assemblages. *S. costatum* aggregates had higher sinking velocities (W_{s-exp} and W_{s-cal}) and twice as many incorporated benthic diatoms compared to aggregates without *S. costatum*. Aggregates with few biological components had 3-fold higher calculated residence times compared to *S. costatum* aggregates and several orders of magnitude shorter than known from the literature.

Aggregates of the latter type will run through a high number of resuspension and deposition loops on their way from the coast to the basin. Cells of benthic diatoms found in surface sediments of both sites will therewith be transported towards the basin. Interactions with the benthic element cycle may then be increased and organic material along with minerals may have a longer retention in coastal sediments.

Literature

- Ackers P, White WR 1973. Sediment Transport: New Approach and analysis. *Journal of the Hydraulic Division of the American Society of Civil Engineers* 99: 2041-2060
- Admiraal W, Peletier H 1979. Influence of organic compounds and light limitation on the growth rate of estuarine benthic diatoms. *British Phycological Journal* 14: 197-206
- Allredge A, Gotschalk C 1988. In situ settling behaviour of marine snow. *Limnology and Oceanography* 33: 339-351
- Allredge AL, Passow U, Logan BE 1993. The abundance and significance of a class of large, transparent organic particles in the ocean. *Deep-Sea Research (Part I)* 40: 1131-1140
- Allredge AL, Silver MW 1988. Characteristics, dynamics and significance of marine snow. *Progress in Oceanography* 20: 41-82
- Amos C, Daborn G, Christian H, Atkinson A, Robertson A 1992. In situ erosion measurements on fine-grained sediments from the Bay of Fundy. *Marine Geology* 108: 175-196
- Amos C, Feeney T, Sutherland T, Luternauer J 1997. The stability of fine-grained sediments from the Fraser River Delta. *Estuarine, Coastal and Shelf Science* 45: 507-524
- Andersen TJ, Jensen KT, Lund-Hansen L, Mouritsen KN, Pejrup M 2002. Enhanced erodibility of fine-grained marine sediments by *Hydrobia ulvae*. *Journal of sea research* 48: 51-58

- Beaulieu SE 2002. Accumulation and fate of phytodetritus on the sea floor. *Oceanography and marine biology: an annual review* 40: 171-232
- Beaulieu SE 2003. Resuspension of phytodetritus from the sea floor: A laboratory flume study. *Limnology and Oceanography* 48: 1235-1244
- Black K, Paterson DM 1997. Measurement of the erosion potential of cohesive marine sediment: A review of current in situ technology. *Journal of Marine Environmental Engineering* 4: 43- 83
- Blanchard G, Paterson DM, Stal LJ, Richard P, Galois R, et al. 2000. The effect of geomorphological structures on potential biostabilisation by microphytobenthos on intertidal mudflats. *Continental Shelf Research* 20: 1243-1256
- Blanchard GF, Sauriau P-G, Cariou-Le Gall V, Gouleau D, Garet M-J, Olivier F 1997. Kinetics of tidal resuspension of microbiota: testing the effects of sediment cohesiveness and bioturbation using flume experiments. *Marine Ecology Progress Series* 151: 17-25
- Bobertz B 2001. Regionalisierung der sedimentären Fazies der südwestlichen Ostsee. Ernst-Moritz-Arndt-Universität Greifswald, PhD Thesis. 1-133 pp.
- Bohling B. 2003. Untersuchungen zur Mobilität natürlicher und anthropogener Sedimente in der Mecklenburger Bucht. Ernst-Moritz-Arndt-Universität Greifswald, PhD Thesis 1-156 pp.
- Cahoon LB 1999. The role of benthic microalgae in neritic ecosystems. *Oceanography and marine biology: an annual review* 37: 47-86
- Christiansen C, Edelvang K, Emeis K, Graf G, Jähmlich S, et al. 2002. Material transport from the nearshore to the basinal environment in the southern Baltic Sea. I. Processes and mass estimates. *Journal of Marine Systems* 35: 133-150
- Christie MC, Dyer KR, Blanchard G, Cramp A, Mitchener HJ, Paterson DM 2000. Temporal and spatial distributions of moisture and organic contents across a macrotidal mudflat. *Continental Shelf Research* 20: 1219-1241

- Daborn G, Amos C, Brylinsky M, Christian H, Drapeau G, et al. 1993. An ecological cascade effect: Migratory birds affect stability of intertidal sediments. *Limnology and Oceanography* 38: 225-231
- Dade WB, Davis JD, Nichols PD, Nowell ARM, Thistle D, et al. 1990. Effects of bacterial exopolymer adhesion on the entrainment of sand. *Geomicrobiology Journal* 8: 1-16
- Dade WB, Hogg JA, Boudreau BP 2001. Physics of flow above the sediment-water interface. In *The Benthic Boundary Layer*, ed. BP Boudreau, BB Joergensen, pp. 4-43. New York: Oxford University Press
- Daemen E 1986. Comparison of methods for the determination of chlorophyll in estuarine sediments. *Netherlands Journal of Sea Research* 20: 21-28
- De Brouwer JFC, Bjelic S, De Deckere EMGT, Stal LJ 2000. Interplay between biology and sedimentology in a mudflat (Biezelingse Ham, Westerschelde, The Netherlands). *Continental Shelf Research* 20: 1159-1177
- De Deckere EMGT, Van de Koppel J, Heip CHR 2000. The influence of *Corophium volutator* abundance on resuspension. *Hydrobiologia* 426: 37-42
- De Jonge VN 1985. The occurrence of "epipsammic" diatom populations: A result of interaction between physical sorting of sediment and certain properties of diatom species. *Estuarine, Coastal and Shelf Science* 21: 607-622
- De Jonge VN, Van den Bergen J 1987. Experiments on the resuspension of estuarine sediments containing benthic diatoms. *Estuarine, Coastal and Shelf Science* 24: 725-740
- De Winder B, Staats N, Stal LJ, Paterson DM 1999. Carbohydrate secretion by phototrophic communities in tidal sediments. *Journal of Sea Research* 2: 131-146
- Decho A. 2000. Microbial biofilms in intertidal systems: an overview. *Continental Shelf Research* 20: 1257-1273

- Decho AW 1990. Microbial exopolymer secretion in ocean environments: their role(s) in webs and marine processes. *Oceanography and marine biology: an annual review* 28: 73-153
- Decho AW, Moriarty DJW 1990. Bacterial exopolymer utilization by a harpacticoid copepod. *Limnology and Oceanography* 35: 1039-1049
- Dera J 1995. Underwater irradiance as a factor affecting primary production. *Dissertations and monographs / Instytut Oceanologii* 7: 1-68
- Dickson R. 1973. The prediction of major Baltic inflows. *Deutsch Hydrographische Zeitschrift* 26: 97-105
- Diercks AR, Asper VL 1997. In situ settling speeds of marine snow aggregates below the mixed layer: Black Sea and Gulf of Mexico. *Deep-Sea Research (Part I)* 44: 385-398
- Eckman JE, Nowell ARM, Jumars PA 1981. Sediment destabilization by animal tubes. *Journal of Marine Research* 39: 361-374
- Edgar LA, Pickett-Heaps JD 1984. Diatom locomotion. *Progress in phycological research* 3: 361-374
- Eisma D 1993. Suspended matter in the aquatic environment. Springer Verlag, Berlin: 1-315 pp.
- Engel A 2000. The role of transparent exopolymer particles (TEP) in the increase in apparent particle stickiness (α) during the decline of a diatom bloom. *Journal of Plankton Research* 22: 485-497
- Engel A, Passow U 2001. Carbon and nitrogen content of transparent exopolymer particles (TEP) in relation to their Alcian Blue adsorption. *Marine Ecology Progress Series* 219: 1-10
- Engel A, Schartau M. 1999. Influence of transparent exopolymer particles (TEP) on sinking velocity of *Nitzschia closterium* aggregates. *Marine Ecology Progress Series* 182: 69-76

- Fowler SW, Knauer GA 1986. Role of large particles in the transport of elements and organic compounds through the oceanic water column. *Progress in Oceanography* 16: 147-194
- Friedrichs M. 2003. Flow-induced effects of macrozoobenthic structures on the near-bed sediment transport. Universität Rostock, PhD Thesis, 1-80 pp.
- Gerdol V, Hughes RG 1994. Feeding behaviour and diet of *Corophium volutator* in an estuary in southeastern England. *Marine Ecology Progress Series* 114: 103-108
- Gibbs RJ 1985. Estuarine flocs: Their size, settling velocity and density. *Journal of Geophysical Research* 90: 3249-3251
- Glud RN, Kuehl M, Wenzhoefer F, Rysgaard S 2002. Benthic diatoms of a high Arctic fjord (Young Sound, NE Greenland): Importance for ecosystem primary production. *Marine ecology progress series* 238: 15-29
- Graf G 1992. Benthic-pelagic coupling: A benthic view. *Oceanography and marine biology: an annual review* 30: 149-190
- Graf G, Rosenberg R 1997. Bioresuspension and biodeposition: A review. *Journal of Marine Systems* 11: 269-278
- Grant J, Bathmann U, Mills E 1986. The interaction between benthic diatom films and sediment transport. *Estuarine, Coastal and Shelf Science* 23: 239-261
- Grant J, Mills E, Hopper C 1986 b. A chlorophyll budget of the sediment-water interface and the effect of stabilizing biofilms on particle fluxes. *Ophelia* 26: 207-219
- Grant J, Bathmann UV 1987. Swept away: resuspension of bacterial mats regulates benthic - pelagic exchange of sulfur. *Science* 236: 1472-1474
- Grant J, Gust G 1987. Prediction of coastal sediment stability from photopigment content of mats of purple sulphur bacteria. *Nature* 330: 224-246
- Gust G 1987. Verfahren und Vorrichtung zum Erzeugen von definierten Bodenschubspannungen. *Patentschrift DE 3717969 C1* Deutsches Patentamt
- Gust G, Morris M 1989. Erosion thresholds and entrainment rates of undisturbed in situ sediments. *Journal of Coastal Research* 5: 87-99

- Gust G, Müller V 1997. Interfacial hydrodynamics and entrainment functions of currently used erosion devices. In *Cohesive Sediments*, ed. N Burt, R Parker, J Watts, John Wiley & Sons Ltd.: 149-174
- Gustafsson N 1993. The HIRLAM 2 final report. *HIRLAM Technical Report 9*, Swedish Meteorological and Hydrographical Institute, Norrköping
- Hamm CE 2002. Interactive aggregation and sedimentation of diatoms and clay-sized lithogenic material. *Limnology and Oceanography* 47: 1790-1795
- HELCOM 1986. Water Balance of the Baltic Sea. *Baltic Sea Environment Proceedings*, Helsinki, Finland
- Hill PS, Mc Cave IN 2001. Suspended particle transport in Benthic Boundary Layer. In *The Benthic Boundary Layer*, ed. BP Boudreau, BB Joergensen, New York: Oxford University Press.: 78-98
- Hjulström, F 1935. Studies in the morphological activity of rivers as illustrated by the river Fyris. Bulletin of the *Geological Institution of the University of Uppsala*: 221-528
- Holland AF, Zingmark RG, Dean JM 1974. Quantitative evidence concerning the stabilization of sediment by marine benthic diatoms. *Marine Biology* 27: 191-196
- Holm-Hansen O, Lorenzen CJ, Holmes RW, Strickland JDH 1965. Fluorometric determination of chlorophyll. *Journal du Conseil international pour l'Exploration de la Mer* 30: 3-15
- Jackson GA. 1990. A model of the formation of marine algal flocs by physical coagulation processes. *Deep-Sea Research (Part I)* 37: 1197-1211
- Jähmlich S, Graf G 1998. Experimente zur Aggregation bodennaher Partikel aus der Mecklenburger Bucht. *Bodden* 6: 59-75
- Jähmlich S, Lund-Hansen L, Leipe T 2002. Enhanced settling velocities and vertical transport of particulate matter by aggregation in the benthic boundary layer. *Danish Journal of Geography* 102: 37-49

- Jähmlich S, Thomsen L, Graf G 1999. Factors controlling aggregate formation in the benthic boundary layer of the Mecklenburg Bight (western Baltic Sea). *Journal of Sea Research* 41: 245-254
- Jørgensen BB, Revsbech NP 1983. Photosynthesis and structure of benthic microbial mats: microelectrode and SEM studies of four cyanobacterial communities. *Limnology and Oceanography* 28: 1075-93
- Jumars PA, Nowell ARM 1984. Effects on benthos on sediment transport: difficulties with functional grouping. *Continental Shelf Research* 3: 115-130
- Kersten M, Thomsen S, Priebisch W, Garbe-Schoenberg CD 1998. Scavenging and particle residence times determined from super(234)Th/super(238)U disequilibria in the coastal waters of Mecklenburg Bay. *Applied Geochemistry* 13: 339-347
- Kioerboe T, Andersen KP, Dam HG 1990. Coagulation efficiency and aggregate formation in marine phytoplankton. *Marine Biology* 107: 235-245
- Kioerboe T, Hansen JLS 1993. Phytoplankton aggregate formation: Observations of patterns and mechanisms of cell sticking and the significance of exopolymeric material. *Journal of Plankton Research* 15: 993-1018
- Krögel F 1997. Einfluß von Viskosität und Dichte des Seewassers auf Transport und Ablagerung von Wattsedimenten (Langeooger Rückseitenwatt, südliche Nordsee). Fachbereich Geowissenschaften, Universität Bremen: 1-168 pp.
- Krumbein WE, Paterson DM, Stal LJ 1994. Biostabilization of Sediments. Bibliotheks und Informationssystem der Universität Oldenburg: 1-522 pp.
- Laima J, Lund-Hansen L, Pazdro K, Christiansen C, Emeis K 1999. Near-bottom fluxes and composition of suspended matter in the Pomeranian Bay (Baltic Sea). *Oceanologia* 41: 335-53
- Lavelle JW, Mofjeld HO 1987. Do critical stresses for incipient motion and erosion really exist? *Journal of Hydraulic Engineering* 113: 370-385

- Leipe T, Loeffler A, Emeis K, Jähmlich S, Bahlo R, Ziervogel K 2000. Vertical Patterns of Suspended Matter Characteristics Along a Coastal-basin Transect in the Western Baltic Sea. *Estuarine, Coastal and Shelf Science* 51: 789-804
- Lemke W, Kuijpers A, Hoffmann G, Milkert D, Atzler R 1994. The Darss Sill, hydrographic threshold in the southwestern Baltic: Late Quaternary geology and recent sediment dynamics. *Continental Shelf Research* 14: 847-870
- Liu D, Wong PTS, Dutka BJ 1973. Determination of carbohydrate in lake sediment by a modified phenol-sulfuric acid method. *Water Research* 7: 741-746
- Lund-Hansen L, Christiansen C, Jensen O, Laima M 1999. The LABEREX chamber for studying the critical shear stress for fine-grained sediment. *Danish Journal of Geography* 99: 1-7
- Lund-Hansen LC, Laima JM, Mouritsen KN, Lam NN, Hai DN 2002. Effects of benthic diatoms, fluff layer, and sediment conditions on critical shear stress in a non-tidal coastal environment. *Journal of the Marine Biological Association, U.K.* 82: 3855/1-8
- Maa J, Sanford L, Halka J 1998. Sediment resuspension characteristics in Baltimore Harbor, Maryland. *Marine Geology* 146: 137-145
- MacIntyre HL, Geider RJ, Miller DC 1996. Microphytobenthos: The ecological role of the "secret garden" of unvegetated, shallow-water marine habitats. 1. Distribution, abundance and primary production. *Estuaries* 19: 186-201
- Madsen K, Nilsson P, Sundbaeck K 1993. The influence of benthic microalgae on the stability of a subtidal sediment. *Journal of Experimental Marine Biology and Ecology* 170: 159-177
- Matthaeus W, Nausch G. 2001. The hydrographic-hydrochemical of the western and central Baltic Sea in 1999/2000 and during the 1990s. *Meereswissenschaftliche Berichte, Warnemünde* 45: 1-133 pp.
- Meadows A, Meadows PS, Wood DM, Murray JMH 1994. Microbiological effects on slope stability: an experimental analysis. *Sedimentology* 41: 423-435

-
- Meadows PS, Tait J 1989. Modification of sediment permeability and shear strength by two burrowing invertebrates. *Marine Biology* 101: 75-82
- Mehta AJ, Lee SC 1994. Problems in linking the threshold condition for the transport of cohesionless and cohesive sediment grain. *Journal of Coastal Research* 10: 170-177
- Mehta AJ, Partheniades E 1982. Resuspension of deposited cohesive sediment beds. *Proceedings of the 18th Coastal Engineering Conference, ASCE*: 1569-1588
- Miller MC, Mc Cave IN, Komar PD 1977. Threshold of sediment motion under unidirectional currents. *Sedimentology* 24: 507-527
- Mitchener H, Torfs H 1996. Erosion of mud/sand mixtures. *Coastal Engineering* 29: 1-25
- Mouritsen KNM, Lone T, Jensen T 1998. Change of topography and sediment characteristics on an intertidal mud-flat following mass-mortality of the amphipod *Corophium volutator*. *Journal of the Marine Biological Association, U.K.* 78: 1167-1180
- Pacanowski RC 1996. MOM-2 Documentation User's Guide and Reference Manual: 3.2, GFDL, Princeton
- Passow U, Alldredge AL 1995 a. Aggregation of a diatom bloom in a mesocosm: The role of transparent exopolymer particles (TEP). *Deep-Sea Research (Part II)* 42: 99-109
- Passow U, Alldredge AL. 1995 b. A dye-binding assay for the spectrophotometric measurement of transparent exopolymer particles (TEP). *Limnology and Oceanography* 40: 1326-1335
- Passow U, Alldredge AL, Logan BE 1994. The role of particulate carbohydrate exudates in the flocculation of diatom blooms. *Deep-Sea Research (Part I)* 41: 335-357
- Paterson DM 1990. The influence of epipelagic diatoms on the erodibility of an artificial sediment. *Proceedings of the 10th international symposium on living and fossil diatoms, 1998*, ed. H Simola, Joensuu, Finland: 345-355

- Paterson DM 1995. Biogenic structure of early sediment fabric visualized by low-temperature scanning electron microscopy. *Journal of the Geological Society, London* 152: 131-140
- Paterson DM, Black KS 1999. Water flow, sediment dynamics and benthic biology. *Advances in Ecological Research* 29: 155-193
- Pempkowiak J, Beldowski J, Pazdro K, Staniszewski A, Leipe T, Emeis K 2002. The contribution of the fine sediment fraction to the Fluffy Layer Suspended Matter (FLSM). *Oceanologia* 44: 513-327
- Porter KG, Feig YS 1980. The use of DAPI for identifying and counting aquatic microflora. *Limnology and Oceanography* 25: 943-948
- Poulos SE 2001. The contribution of near-bed currents to modern sedimentation processes in the deep water of the Hellenic Arc-Trench system, eastern Mediterranean. *Geo-Marine Letters* 20: 201-208
- Puls W, Kuehl H 1996. Settling velocity determination using the BIGDAN settling tube and the Owen settling tube. *Journal of Sea Research* 36: 119-125
- Riethmueller R, Heineke M, Kuehl H, Keujer-Ruediger R 2000. Chlorophyll *a* concentration as an index of sediment surface stabilisation by microphytobenthos? *Continental Shelf Research* 20: 1351-1372
- Rietz V, Bobertz B, Seifert T, Harff J 2000. Numerical simulations of sediment transport processes caused by currents and waves in the western Baltic Sea. *Abstract Volume Geological Survey of Brazil*, 31st International Geological Congress, Rio de Janeiro
- Saburova M, Polikarpov I 2003. Diatom activity within soft sediments: behavioural and physiological processes. *Marine ecology progress series* 251: 115-126
- Sanford L, Panageotou W, Halka J 1991. Tidal resuspension of sediments in northern Chesapeake Bay. *Marine Geology* 97: 87-103
- Seifert T, Kayser B. 1995. A high resolution spherical grid topography of the Baltic Sea. *Meereswissenschaftliche Berichte, Warnemuende* 9: 72-88

-
- Seifert T, Tauber F, Kayser B. 2001. A high resolution spherical grid topography of the Baltic Sea - revised edition. *Proceedings of the Baltic Sea Science Conference*, Stockholm
- Shanks AL, Edmondson EW 1989. Laboratory-made artificial marine snow: A biological model of the real thing. *Marine Biology* 101: 463-470
- Shields A 1936. Anwendung der Ähnlichkeits-Mechanik und der Turbulenzforschung auf die Geschiebebewegung. *Preussische Versuchsanstalt für Wasserbau und Schiffahrt* 2b, Berlin
- Simon M, Grossart HP, Schweitzer B, Ploug H 2002. Microbial ecology of organic aggregates in aquatic ecosystems. *Aquatic Microbial Ecology* 28: 175-211
- Smetacek VS 1985. Role of sinking in diatom life-history cycles: Ecological, evolutionary and geological significance. *Marine Biology* 84: 239-251
- Smith D, Underwood G 1998. Exopolymer production by intertidal epipelagic diatoms. *Limnology and Oceanography* 43: 1578-1591
- Soulsby RL 1983. The bottom boundary Layer in shelf seas. In *Physical Oceanography of Coastal and Shelf Seas*, ed. B Johns, Amsterdam: Elsevier Oceanography Series: 189 - 266
- Soulsby RL, Whitehouse R 1997. Threshold of sediment motion in coastal environments. *Proceedings of Pacific Coast and Ports conference* 1, University of Canterbury, Christchurch, New Zealand: 149-154
- Soulsby RL 1997. Dynamics of marine Sands: A manual for practical applications. Thomas Telford Publications: 1-249 pp.
- Springer BM 1999. Modifikation des bodennahen Strömungsregimes und die Deposition von suspendiertem Material durch Makrofauna. *Geomar Report* 74: 1-112 pp.
- Staats N, Stal L, de Winder B, Mur L 2000. Oxygenic photosynthesis as driving process in exopolysaccharide production of benthic diatoms. *Marine ecology progress series* 193: 261-269

- Stoderegger K, Herndl GJ 1998. Production and release of bacterial capsular material and its subsequent utilization by marine bacterioplankton. *Limnology and Oceanography* 43: 877-884
- Stoderegger KE, Herndl GJ 1999. Production of exopolymer particles by marine bacterioplankton under contrasting turbulence conditions. *Marine Ecology Progress Series* 189: 9-16
- Stolzenbach K, Newman K, Wong C 1992. Aggregation of fine particles at the sediment-water interface. *Journal of Geophysical Research* 97: 17889-17898
- Sundbaeck K 1984. Distribution of microbenthic chlorophyll-a and diatom species related to sediment characteristics. *Ophelia Suppl.* 3: 229-246
- Sundbaeck K 1986. What are the benthic microalgae doing on the bottom of Laholm Bay? *Ophelia Suppl.* 4: 273-286
- Sundbaeck K, Joensuu B 1988. Microphytobenthic productivity and biomass in sublittoral sediments of a stratified bay, southeastern Kattegat. *Journal of Experimental Marine Biology and Ecology* 122: 63-81
- Sutherland T, Amos C, Grant J 1998. The effect of buoyant biofilms on the erodibility of sublittoral sediments of a temperate microtidal estuary. *Limnology and Oceanography* 43: 225-235
- Thomsen L, Gust G 2000. Sediment erosion thresholds and characteristics of resuspended aggregates on the western European continental margin. *Deep-Sea Research (Part I)* 47: 1881-1897
- Thomsen L, Van Weering TCE 1998. Spatial and temporal variability of particulate matter in the benthic boundary layer at the N.W. European Continental Margin (Goban Spur). *Progress in Oceanography* 42: 1-4
- Thomsen LA, McCave IN 2000. Aggregation processes in the benthic boundary layer at the Celtic Sea continental margin. *Deep Sea Research (Part I)* 47: 1389-1404

- Tolhurst T, Black K, Paterson D, Mitchener H, Termaat G, Shayler S 2000. A comparison and measurement standardisation of four in situ devices for determining the erosion shear stress of intertidal sediments. *Cont. Shelf Res.* 20: 1397-1418
- Turnewitsch R, Graf G 2003. Variability of particulate seawater properties related to bottom mixed layer-associated internal waves in shallow water on a time scale of hours. *Limnology and Oceanography* 48: 1254-1264
- Turnewitsch R, Springer BM 2001. Do bottom mixed layers influence super(234)Th dynamics in the abyssal near-bottom water column? *Deep Sea Research (Part I)* 48: 1279-1307
- Underwood GJC, Paterson DM 1993. Recovery of intertidal benthic diatoms after biocide treatment and associated sediment dynamics. *Journal of the Marine Biological Association, U.K.* 73: 25- 45
- Underwood GJC, Paterson DM, Parkes RJ 1995. The measurement of microbial carbohydrate exopolymers from intertidal sediments. *Limnology and Oceanography* 40: 1243-1253
- Underwood GJC, Smith DJ 1998. Predicting epipelagic diatom exopolymer concentrations in intertidal sediments from sediment chlorophyll *a*. *Microbial Ecology* 35: 116-125
- UNESCO 1994. Protocols for the joint global ocean flux study (JGOFS) core measurements. In *Intergovernmental oceanographic commission and Scientific Committee on oceanic research*. Bergen, Norway
- Utermöhl H 1958. Zur Vervollkommnung der quantitativen Phytoplankton-Methodik. *Internationale Vereinigung für Theoretische und Angewandte Limnologie* 9: 1-38
- Van Duyl F, De Winder B, Kopa A, Wollenzien U 2000. Consequences of diatom mat erosion for carbohydrate concentrations and heterotrophic bacterial activities in intertidal sediments of the Ems-Dollard estuary. *Continental Shelf Research* 20: 1335-1349

- Vandevivere P, Kirchman DL 1993. Attachment stimulates exopolysaccharide synthesis by a bacterium. *Applied and Environmental Microbiology*: 3280 - 3286
- Von Bodungen B, Wunsch M, Fuderer H. 1991. Sampling and analysis of suspended and sinking particles in the northern North Atlantic. In *Marine particles: analysis and characterization*, ed. DC Hurd, DW Spencer, Washington DC, American Geophysical Union: 47-56
- Walsby AE 1997. Numerical integration of phytoplankton photosynthesis through time and depth in a water column. *New Phytologist* 136: 189-209
- Wasmund N, Nausch G, Matthaeus W 1998. Phytoplankton spring blooms in the southern Baltic Sea--spatio-temporal development and long-term trends. *Journal of Plankton Research* 20: 1099-1117
- Widdows J, Brinsley MD 2002. Impact of biotic and abiotic processes on sediment dynamics and the consequences to the structure and functioning of the intertidal zone. *Journal of Sea Research* 78: 143-156
- Wiltshire KH 2000. Algae and associated pigments of intertidal sediments, new observations and methods. *Limnologica* 30: 205-214
- Wiltshire KH, Tolhurst T, Paterson DM, Davidson I, Gust G. 1998. Pigment fingerprints as markers of erosion and changes in cohesive sediment surface properties in simulated and natural erosion events. In *Sedimentary processes in intertidal zones*, ed. KS Black, DM Paterson, A Cramp, Geological Society, London: 99 - 114
- Witt G, Leipe T, Emeis KC. 2001. Using Fluffy Layer Material To Study the Fate of Particle-Bound Organic Pollutants in the Southern Baltic Sea. *Environmental Science & Technology* 35: 1567-1573
- Wright LD 1989. Benthic boundary layers of estuarine and coastal environments. *Reviews in Aquatic Sciences* 1: 75-95
- Yallop ML, Paterson DM, Wellsbury P 2000. Interrelationships between rates of microbial production, exopolymer production, microbial biomass, and sediment stability in biofilms of intertidal sediments. *Microbial Ecology* 39: 116-27

-
- Zanke U 1977. Neuer Ansatz zur Berechnung des Transportbeginns von Sedimenten unter Strömungseinfluss. Mitteilungen des Franzius-Instituts, Universität Hannover 46: 156-178
- Zanke U 1982. Grundlagen der Sedimentbewegung. Springer Verlag, Berlin: 1-402 pp.
- Zettler ML, Bönsch R, Gosselck F 2000. Verbreitung des Makrozoobenthos in der Mecklenburger Bucht (südliche Ostsee) - rezent und im historischen Vergleich. *Meereswissenschaftliche Berichte, Warnemünde* 42: 1-144 pp.

Danksagung

Recht herzlich bedanken möchte ich mich bei Herrn Prof. Dr. Gerhard Graf, der die Begutachtung meiner Arbeit übernommen hat.

Außerdem gilt mein Dank Herrn Prof. Dr. Jan Harff, der als Leiter und Koordinator des vom BMBF finanzierten Projektes DYNAS die Durchführung und Fertigstellung dieser Arbeit ermöglicht hat.

Meinen Kollegen und Mitstreitern Robert Turnewitsch (SOC), Florian Peine, Michael Friedrichs (Uni Rostock) und Björn Bohling danke ich für die gute Arbeitsatmosphäre im Laufe der drei Jahre DYNASTIE I. Das nette Arbeitsklima an Bord der FS A. v. Humboldt und FS Prof. A. Penck haben natürlich in großem Maße zum Gelingen der Arbeit beigetragen. Die Reisen werden mir natürlich immer in Erinnerung bleiben! DANKE!

Im Institut für Ostseeforschung Warnemünde fand ich immer große Unterstützung und möchte mich daher bei den Mitarbeitern, Kollegen und Freunden herzlich bedanken.

Mein besonderer Dank gilt meiner Familie in Büsum, Eutin und Langwedel, die mich im Laufe meines Studiums und während der Promotion immer unterstützt haben, in welcher Form auch immer!

Last but not least: Danke Stefan!!! Ohne Deine Unterstützung wäre mir diese Arbeit sicher nicht gelungen, vielen Dank!

Erklärung

Hiermit versichere ich, dass ich die vorliegende Arbeit selbständig angefertigt und ohne fremde Hilfe verfasst habe, keine außer den von mir angegebenen Hilfsmittel und Quellen dazu verwendet habe und die den benutzten Werken inhaltlich und wörtlich entnommen Stellen als solche kenntlich gemacht habe.

Rostock, den 24.09.2003

(Kai Ziervogel)

Lebenslauf

Persönlich Daten

Name, Vorname: Ziervogel, Kai

Adresse: Kopernikusstrasse 15, 18057 Rostock

Geburtsdatum: 25. Februar 1972

Geburtsort: Heide in Holstein

Schulbildung

Juni 1991: Abitur am Nordsee-Gymnasium-Büsum

Zivildienst

Juni 1991 – August 1992: Schutzstation Wattenmeer e.V. in Büsum

Hochschulausbildung

- Sommersemester 1993: Immatrikulation an der Fachhochschule Flensburg im Fachbereich Maschinenbau
- Wintersemester 1993/94: Immatrikulation an der Universität Kaiserslautern im Fachbereich Biologie
- September 1995: Diplom - Vorprüfung für Biologen an der Universität Kaiserslautern
- Wintersemester 1995/96: Immatrikulation an der Universität Rostock zum Hauptstudium der Biologie
- Wintersemester 1996/97: Auslandssemester an der Universität Reading (England)
- Wintersemester 1999/00: Beendigung des Biologiestudiums mit der Verleihung des akademischen Grades: Diplombiologe
- Sommersemester 2000: Beginn der Promotion am Institut für Ostseeforschung Warnemünde in der Sektion Biologische Meereskunde
- Wintersemester 2000: Rostocker Wissenschaftspreis 2000

Berufstätigkeit

- Seit Juli 2000: Wissenschaftlicher Angestellte am Institut für Ostseeforschung Warnemünde